Ore Geology Reviews 73 (2016) 127–147

Contents lists available at ScienceDirect

Ore Geology Reviews

journal homepage: www.elsevier.com/locate/oregeorev

Critical metals (REE, Sc, PGE) in Ni laterites from Cuba and the Dominican Republic

Thomas Aiglsperger [a,*], Joaquin A. Proenza [a], John F. Lewis [b], Manuel Labrador [a], Martin Svojtka [c], Arturo Rojas-Purón [d], Francisco Longo [e], Jana Ďurišová [c]

[a] Departament de Cristal·lografia, Mineralogia i Dipòsits Minerals, Universitat de Barcelona (UB), Martí i Franquès s/n, 08028 Barcelona, Spain
[b] Department of Earth and Environmental Sciences, The George Washington University, Washington, DC 20052, USA
[c] Institute of Geology, Academy of Sciences, v.v.i., Rozvojova´ 269, 16500 Praha 6, Czech Republic
[d] Departamento de Geología, Instituto Superior Minero Metalúrgico de Moa, Las Coloradas s/n, Moa, Holguín, Cuba
[e] Falcondo Glencore Nickel, Box 1343, Santo Domingo, Dominican Republic

ARTICLE INFO

Article history:
Received 10 April 2015
Received in revised form 29 September 2015
Accepted 8 October 2015
Available online 13 October 2015

Keywords:
Ni laterite
Rare Earth Elements
Scandium
Platinum Group Elements
Moa Bay mining area
Falcondo mining area
Cuba
Dominican Republic
Caribbean

ABSTRACT

Ni laterites are considered worthy targets for critical metals (CM) exploration as Rare Earth Elements (REE), Sc and platinum group elements (PGE) can be concentrated during weathering as a result of residual and secondary enrichment. In this contribution geochemical and mineralogical data of CM from two different nickel laterite types (i) from the Moa Bay mining area in Cuba (oxide type) and (ii) from the Falcondo mining area in the Dominican Republic (hydrous Mg silicate type) are presented. Emphasis is given on examining their potential to accumulate CM and on processes involved. Results show that CM are concentrated towards the surface in specific zones: (i) REE in clay minerals rich horizons and within zones composed of secondary Mn oxide(s), (ii) Sc within zones rich in secondary Fe and Mn bearing oxide(s) and (iii) PGE in zones with high concentrations of residual chromian spinel and secondary Fe and Mn bearing oxide(s) at upper levels of the Ni laterite profiles. Concentration factors involve (i) residual enrichment by intense weathering, (ii) mobilization of CM during changing Eh and pH conditions with subsequent reprecipitation at favourable geochemical barriers and (iii) interactions between biosphere and limonitic soils at highest levels of the profile (critical zone) with involved neoformation processes. Total contents of CM in both Ni laterite types are low when compared with conventional CM ore deposits but are of economic significance as CM have to be seen as cost inexpensive by-products during the Ni (+Co) production. Innovative extraction methods currently under development are believed to boost the significance of Ni laterites as future unconventional CM ore deposits.

1. Introduction

The Rare Earth Elements (REE), Platinum Group Elements (PGE) and scandium (the so-called "High Tech metals") are elements with special chemical and physical properties needed for sophisticated technical applications associated with renewable energy, reduction of greenhouse gases and energy efficiency (green technologies). The rapidly growing market in this sector (e.g. production of permanent magnets, cell phones, electric cars, wind turbines) led to an increasing demand of these metals over the last few years (e.g. Chakhmouradian and Wall, 2012; Hein et al., 2013). In 2014, the EU Commission assessed 54 materials (metallic ore, biotic material and industrial minerals) on their criticality for Europe's industry on the basis of their high economic importance and their high relative supply risk (EC, 2014). 20 raw materials were identified as critical including REE and PGE.

In 2010, the unexpected drastic reduction of export quotas for REE by the Chinese government revealed the vulnerability of western high tech industries. As a consequence, new exploration projects have been initiated worldwide. However, to be competitive these deposits must be large in scale, easily accessible (open pit mining) with favourable ore mineralogy from a metallurgical point of view and tolerable environmental impact. With respect to PGE, being essential for gasoline-engine catalytic converters in the car industry and in other high tech applications, an estimated 82% of the currently mined PGE come from only two major ore deposits in South Africa (Bushveld complex) and Russia (Norilsk) (USGS, 2013). Supply risks and price instabilities can occur when producers suffer full-scale mine shutdowns as seen during several strikes held by mining workers in South Africa 2013 (USGS, 2013), or when political environments change in times of crisis (e.g. 2015 EU–Russia sanctions during Ukraine crisis).

Ore deposits associated with near-surface modification of ultramafic rocks could help to minimize supply risks of these critical metals (CM) (e.g. Wilde et al., 2003). Ni laterites are considered worthy targets for CM exploration as REE, Sc and PGE can be concentrated during

* Corresponding author.
E-mail address: thomas.aiglsperger@ub.edu (T. Aiglsperger).

http://dx.doi.org/10.1016/j.oregeorev.2015.10.010
0169-1368/

weathering as a result of residual and secondary enrichment (e.g. Maksimović and Pantó, 1996; Economou-Eliopoulos et al., 1997; Eliopoulos and Economou-Eliopoulos, 2000; Audet, 2008; Ndjigui and Bilong, 2010; Wang et al., 2011; Eliopoulos et al., 2014). In addition, changing Eh–pH conditions at higher levels of the laterite profile and subsequent interactions within the biosphere can favour mobility, reprecipitation and concentration of these elements (Aiglsperger et al., 2015).

Ni (±Co) laterite deposits account for about 60% of the current world's annual Ni production and host 60 to 70% of the world land-based Ni resources (Butt and Cluzel, 2013). In this context Cuba and the Dominican Republic host some of the world's most important Ni laterite deposits. They formed by weathering of ophiolitic serpentinized peridotites in the Tertiary as a result of tropical climate conditions (e.g. Linchenat and Shirakova, 1964; Haldemann et al., 1979; Lithgow, 1993; Lavaut, 1998; Lewis et al., 2006a). They have been mined since 1943 when the Nicaro processing plant (eastern Cuba) went into production (Nelson et al., 2011). The Ni laterite deposits currently being mined are located in eastern Cuba (Moa Bay mining area) and the central Dominican Republic (Falcondo mining area). According to the mineralogy of principal ore-bearing phases, the Moa Bay ore deposits are classified as oxide type, and Falcondo ore deposits as hydrous Mg silicate type (Brand et al., 1998; Lewis et al., 2006a).

In this work, geochemical and mineralogical data from two different nickel laterite types (i) from the Moa Bay mining area (eastern Cuba) and (ii) from the Falcondo mining area (Dominican Republic) is presented, with emphasis on their potential to accumulate CM and on processes involved. Data and behaviour of the most abundant CM in Ni laterites, cobalt, are discussed in a separate publication currently under development and continues with previous work from the study area (Labrador et al., 2007; Proenza et al., 2010; Roqué-Rosell et al., 2010). The underlying idea of this investigation is that here discussed CM could be produced as by-products additionally to approximately 130,000 t of Ni annually produced in active plants in the Caribbean (Nelson et al., 2011).

2. Geological setting

The Ni laterites from the Moa Bay and Falcondo mining areas are located in the northern Caribbean (Fig. 1). They are developed on ophiolite complexes with serpentinized peridotite that crop out as tectonic belts along the margins of the Caribbean plate (Lewis et al., 2006a). However, eastern Cuba and the central Dominican Republic contain the largest ore deposits.

2.1. The Moa Bay mining area

Ni laterites of the Moa Bay mining area form part of an ~100 km^2 large Ni laterite province in the northeast of Cuba (Pinares de Mayarí, Nicaro and Moa Bay mining areas), making it one of the largest reserves of nickel and cobalt in the world (Linchenat and Shirakova, 1964; Lavaut, 1998; Lewis et al., 2006a; Fig. 2a, b). According to Beaton et al. (2011) measured and indicated metal resources were 66.60 Mt at 1.26% Ni and 0.13% Co in 2010. Proven and probable reserves of 47.77 Mt with a grade of 1.19% Ni and 0.13% Co were reported by the same authors. The Moa Bay Ni laterites have developed from weathering of hydrated ultramafic rocks of the Moa–Baracoa ophiolitic massif. This massif form the eastern part of the Mayarí–Baracoa ophiolitic belt in northeastern Cuba (Proenza et al., 1999a,b; Marchesi et al., 2006) and consists of mantle tectonites (>2.2 km) followed by a thin (~300 m) crustal section of lower gabbros and discordant basaltic rocks with back arc basin affinity (Iturralde-Vinent et al., 2006; Marchesi et al., 2006; Proenza et al., 2006). The ultramafic rocks are mainly harzburgites (more than 70%) and lesser amounts of dunites. Concordant and subconcordant bodies of dunite, sills of gabbro and chromitite bodies within a dunite envelope are also present. The degree of serpentinization is most in shear or fracture zones, where it reaches a maximum value of 95% relative to the whole rock (typical serpentinite). The peridotites are cut by dikes of gabbro, pegmatite gabbro, olivine norite and minor pyroxenite (Proenza et al., 1999a,b; Marchesi et al., 2006). The emplacement of the ophiolite took place in the Maastrichtian to early Danian with weathering, lateritization and subsequent ore deposit formation commencing during the Miocene (Iturralde-Vinent et al., 2006; Lewis et al., 2006a).

The Moa Bay Ni laterite mining area is classified as oxide type (Brand et al., 1998; Gleeson et al., 2003) and is divided into 9 ore deposits: Moa Occidental, Moa Oriental, Punta Gorda, Yagrumaje, Camarioca Norte, Camarioca Sur, La Delta, Cantarrana, and Santa Teresita (e.g. Lavaut, 1998) producing at least 34.263 t of Ni and 3.792 t of Co in 2012 (Sherritt, 2012).

The laterite profile at Moa Bay has been divided into various zones and subzones by mine workers and Cuban geologists but the nomenclature of these zones does not follow the recommended classification for

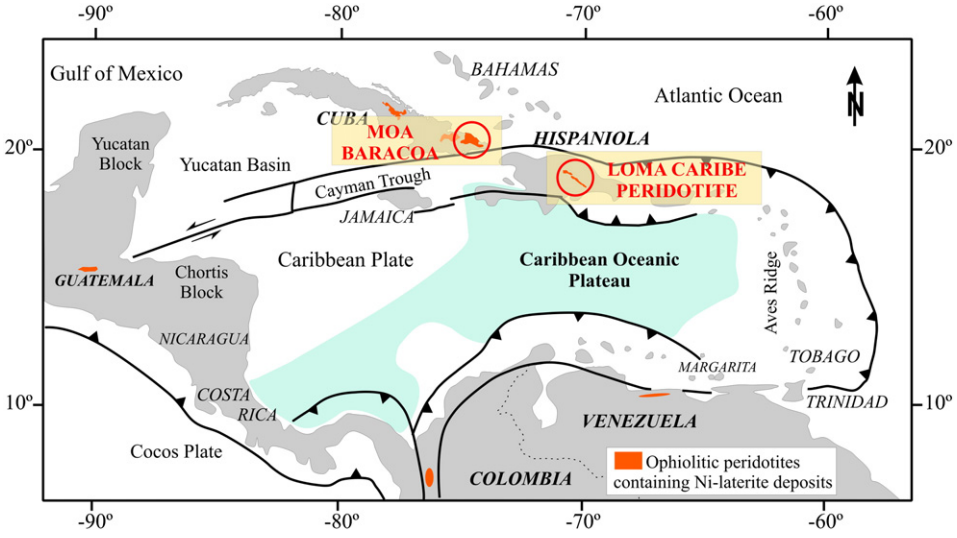

Fig. 1. Distribution of ophiolitic peridotites containing Ni laterite deposits around the margins of the Caribbean Plate; Ni laterite deposits from Moa Baracoa (Cuba) and from the Loma Caribe peridotite (Dominican Republic) are highlighted.
Modified from Lewis et al. (2006a).

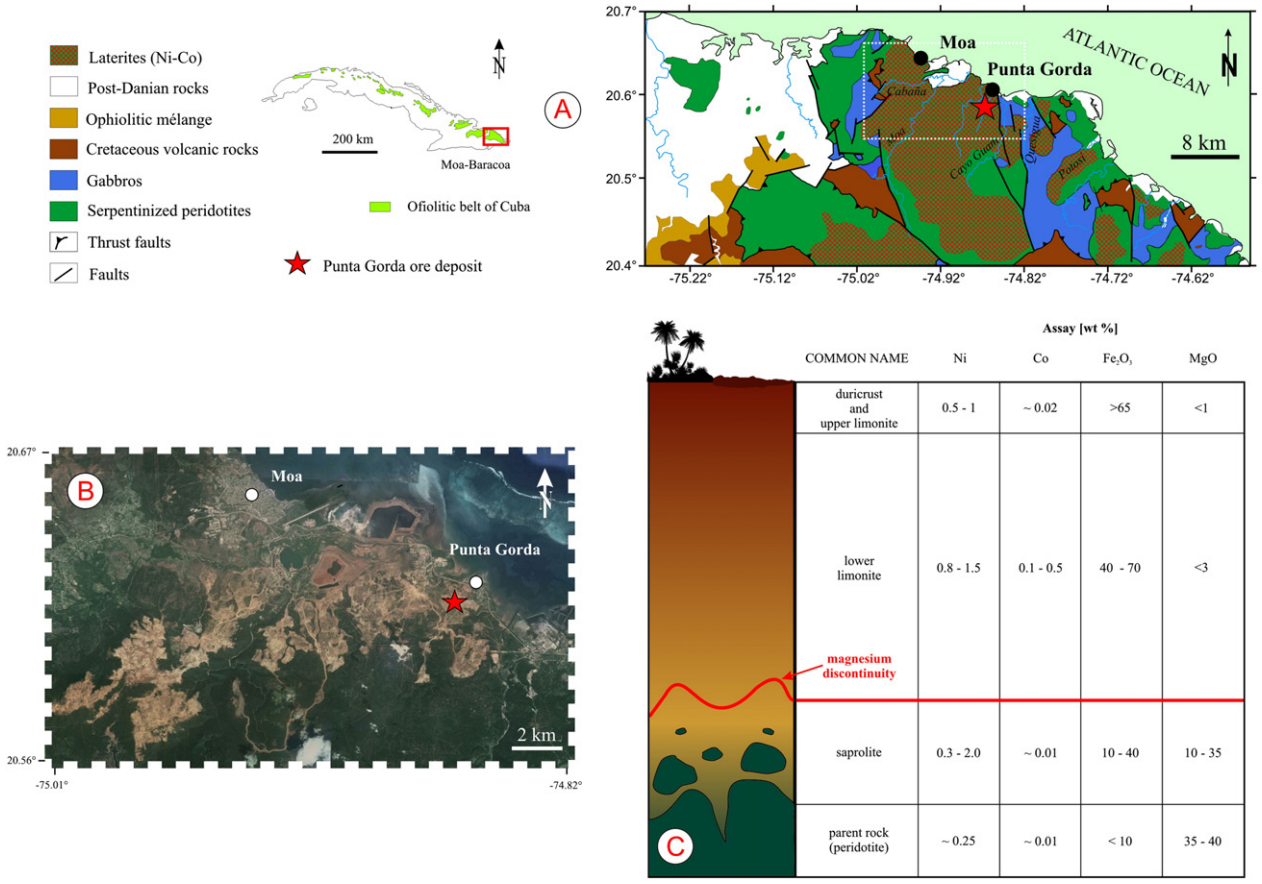

Fig. 2. A) Geographic location and simplified geological map of the Cuban study area (Moa Baracoa) showing the location of the Punta Gorda ore deposit. B) Orthophotograph showing the Moa Bay mining area with the Punta Gorda ore deposit. C) Idealized Ni laterite soil profile from Moa Bay ore deposits with characteristic assay results.
Panel A modified from Marchesi et al. (2006).

Ni laterite deposits (e.g. Lavaut, 1998; Proenza et al., 2007a; Golightly, 2010). In general five horizons can be recognized from bottom to top that have been described in other Ni laterite deposits of the world: (i) parent rock peridotite, (ii) saprolite, (iii) lower limonite, (iv) upper limonite, and (v) duricrust (Fig. 2c). Within the profile pale bauxitic zones of weathered gabbro (up to 5 m thick) are abundant. As typical in oxide type Ni laterite deposits the limonite horizons above the magnesium discontinuity (Butt and Cluzel, 2013) are dominant and can reach a total thickness of more than 50 m in the laterite profile. Moa Bay deposits usually lack hydrous Mg silicate rich saprolite horizons beneath the magnesium discontinuity, however, the thicker profiles have saprolite roots (Golightly et al., 2008).

The ore minerals are mainly goethite (~1.4 wt.% Ni), minor maghemite (up to ~8 wt.% Ni), lithiophorite (~8.1 wt.% Ni, ~4.5 wt.% Co) and "lithiophorite–asbolane intermediate" (up to 22 wt.% Ni), which all occur in the limonite horizon of the profile (Proenza et al., 2007a; Roqué-Rosell et al., 2010).

2.2. The Falcondo mining area

Located in the central part of the Dominican Republic the Falcondo mining area contains the largest hydrous Mg silicate type Ni laterite deposits of the Caribbean with measured and indicated Ni resources of 67.8 Mt at a grade of 1.5% Ni plus 4.9 Mt at 1.4% Ni inferred (Redwood, 2014). The Falcondo mining area is divided into 7 ore deposits: Loma Peguera, Loma Larga, Loma Cumpié, Loma Guardarraya, Loma Caribe, Loma Ortega and Loma Miranda (Haldemann et al., 1979; Lithgow, 1993; Lewis et al., 2006a).

The Ni laterite at Falcondo developed over the so called Loma Caribe peridotite which occurs as a serpentinized belt of ultramafic rocks approximately 4–5 km wide and 95 km long in the NW of Santo Domingo (Fig. 3a, b). The Loma Caribe peridotite is accompanied by two major metavolcanic units: 1) the Maimón Formation in the NE representing a primitive island arc tholeiitic unit of Lower Cretaceous age, and 2) the Duarte Complex in the SW representing mantle plume-related oceanic plateau basalts of Late Jurassic or at least Early Cretaceous age (Lewis et al., 2002, 2006b; Escuder Viruete et al., 2007). Both units are unconformably overlain: the Maimón Formation by the Peralvillo Formation (volcanic arc andesites, diorites, basalts, tuffs, breccias and conglomerates of Late Cretaceous age) and the Duarte Complex by the Siete Cabezas Formation (volcanic arc basalts with minor tuffs and wackes of Cenomanian age) (Haldemann et al., 1979; Lewis et al., 2002; Proenza et al., 2007b). Dolerite and micro gabbro dikes occur within the peridotite belt and diorite bodies outcrop along its faulted margins (Lithgow, 1993; Escuder Viruete et al., 2006). According to Lewis and Jiménez (1991) the mineralogy and textural features of the ultramafic rocks indicate that the Loma Caribe peridotite represents (serpentinized) harzburgitic oceanic mantle as part of a dismembered ophiolite complex. Recent geochemical studies reveal that the ultramafic rocks were formed as an evolving suprasubduction oceanic lithosphere (Lewis et al., 2006a; Marchesi et al., 2012) and have been partially serpentinized by hydrothermal reaction with sea water and by hydrothermal reactions during emplacement. The emplacement of the peridotites is believed to have been due to the collision of an oceanic plateau (Duarte terrane) with the primitive Caribbean island arc (Maimon–Amina–Los Ranchos terrane) resulting in thrusting of the peridotites in a northerly direction as early as late Albian (Draper et al., 1996; Lewis et al., 2002, 2006a).

Starting from early Miocene weathering has formed well-developed Ni laterites in the Caribbean showing similar features as other ophiolite-related hydrous Mg silicate Ni deposits found and exploited in the arcs

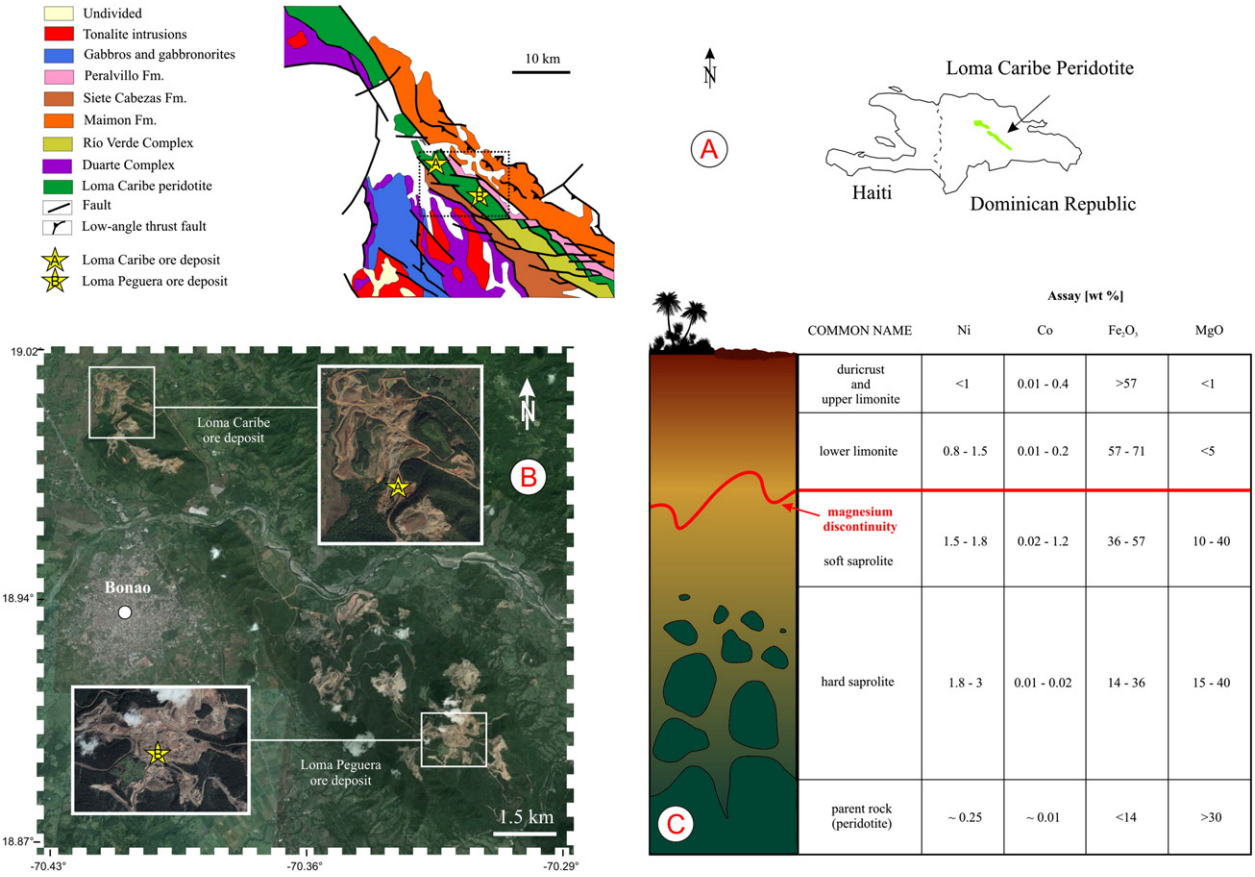

Fig. 3. A) Geographic location and simplified geological map of the central section of the Loma Caribe peridotite showing the location of the Loma Caribe and Loma Peguera ore deposits. B) Orthophotograph showing the Falcondo mining area with Loma Caribe and Loma Peguera ore deposits. C) Idealized Ni laterite soil profile from Falcondo ore deposits with characteristic assay results.
Panel A modified from Bowin (1966) and Escuder Viruete et al. (2007).

of the West Pacific (Golightly, 2010; Butt and Cluzel, 2013; Villanova-de-Benavent et al., 2014). Mine geologists of Falcondo have subdivided and named the weathering profile into several zones (A–F) on the basis of Ni, Mg and Fe contents, textures and mineralogy (Haldemann et al., 1979; Lithgow, 1993; Lewis et al., 2006a; Villanova-de-Benavent et al., 2014; Aiglsperger et al., 2015). However, to simplify comparison with the investigated Ni laterite profile of Moa Bay the laterite profile of Falcondo was termed from bottom to top: (i) parent rock peridotite, (ii) hard saprolite, (iii) soft saprolite, (iv) lower limonite, and (v) upper limonite and duricrust (Fig. 3c). Ore minerals are mainly Ni-lizardite and poorly defined varieties of Ni containing serpentine, talc, chlorite and sepiolite, commonly termed as "garnierites" (up to 49 wt.% NiO). These are found mainly within the lower part of the saprolite horizon (Villanova-de-Benavent et al., 2014).

It is pointed out, that in both Ni laterite mining areas (i.e. Moa Bay and Falcondo) weathering horizons are erratically developed and complete profiles as shown in Figs. 2c and 3c are extremely rare. Fig. 4 shows some field impressions (see also Fig. 2 in Aiglsperger et al., 2015).

3. Analytical methods

3.1. Sample selection

3.1.1. Moa Bay

Nine samples (~1 kg each) were collected from different levels in one Ni laterite profile approximately 3 km to the south of Punta Gorda (Figs. 2a, b, 5). The profile is ~40 m thick and consists of a 2 m thick

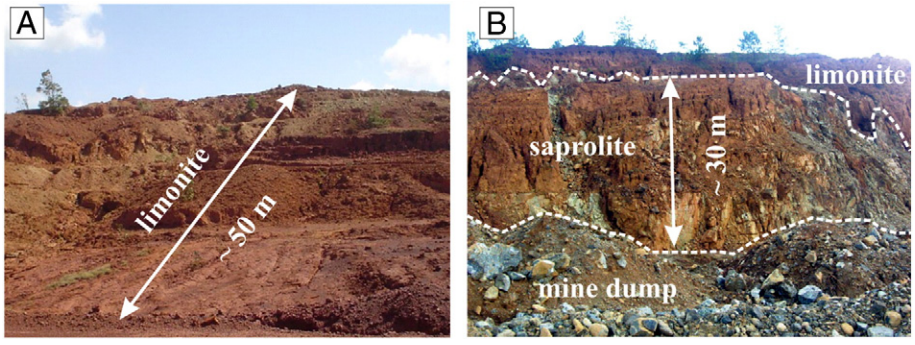

Fig. 4. Characteristic field observations of A) limonite horizon dominated ore deposits from the Moa Bay mining area and B) saprolite horizon dominated ore deposits from the Falcondo mining area.

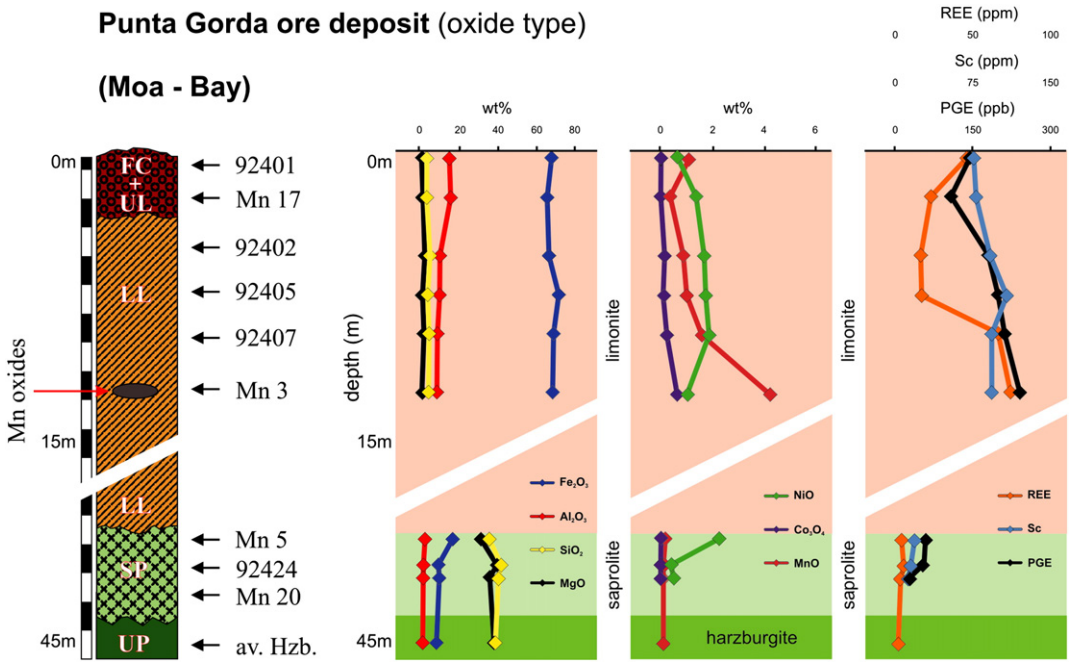

Fig. 5. Ni laterite profile from the Punta Gorda ore deposit (Moa Bay) showing location of samples with major, relevant minor and CM contents. Values for the parent rock (harzburgite) *av. Hzb.* are taken from Marchesi et al. (2006).

layer of duricrust and upper limonite, a 33 m thick package of lower limonite including zones rich in Mn oxide(s) and a 5 m thick zone of soft and hard saprolite overlying serpentinized peridotite (Fig. 5). Parent rocks of Ni laterites from Moa Bay are mainly unweathered harzburgite which have been analysed previously by Marchesi et al. (2006). Average values of unweathered harzburgite from this publication were taken for this investigation.

3.1.2. Falcondo

Two Ni laterite profiles, approximately 13 km apart, were studied, i.e. Loma Caribe and Loma Peguera (Fig. 3a, b). At Loma Caribe 9 samples (~3 kg each) were collected from different levels of a 16 m thick weathering profile consisting of 2 m upper limonite including an about 10 cm thick layer of clay minerals, 5 m lower limonite, 8 m soft and hard saprolite, 1 m serpentinized peridotite and underlying unweathered dunite (Fig. 6).

At Loma Peguera the 16 m thick weathering profile is characterized by a 2 m thin cover of upper limonite underlain by 13 m of saprolite including rare chromitite bodies a few metres thick, overlying dunites (Fig. 7). In total eight characteristic samples (~3 kg each) from indicated horizons were collected for this investigation (Fig. 7).

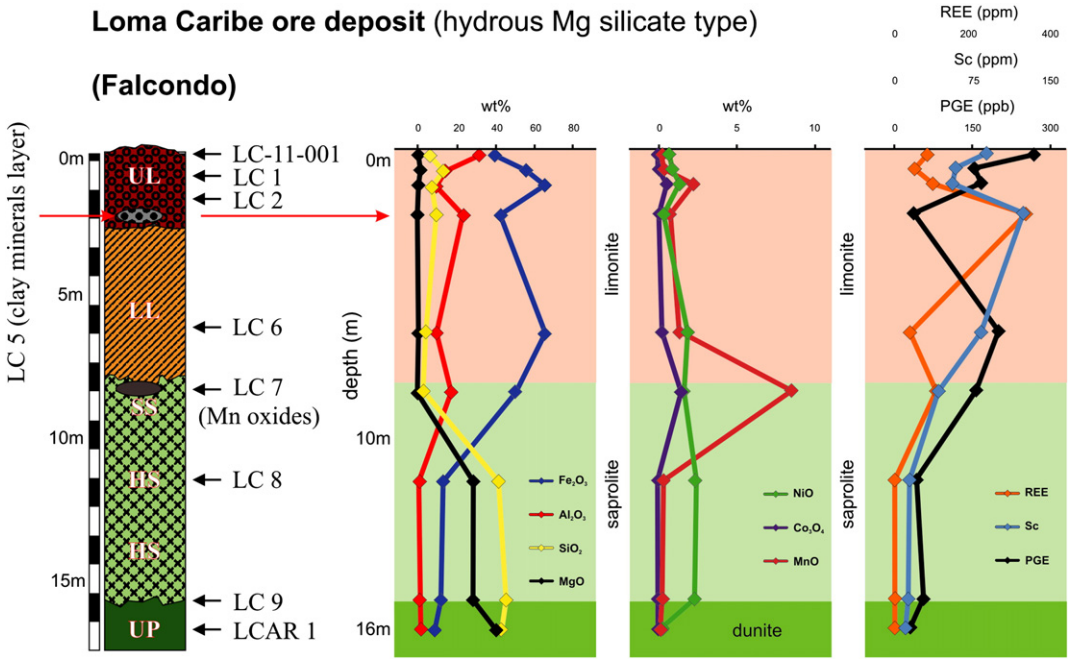

Fig. 6. Ni laterite profile from the Loma Caribe ore deposit (Falcondo) showing location of samples with major, relevant minor and CM contents.

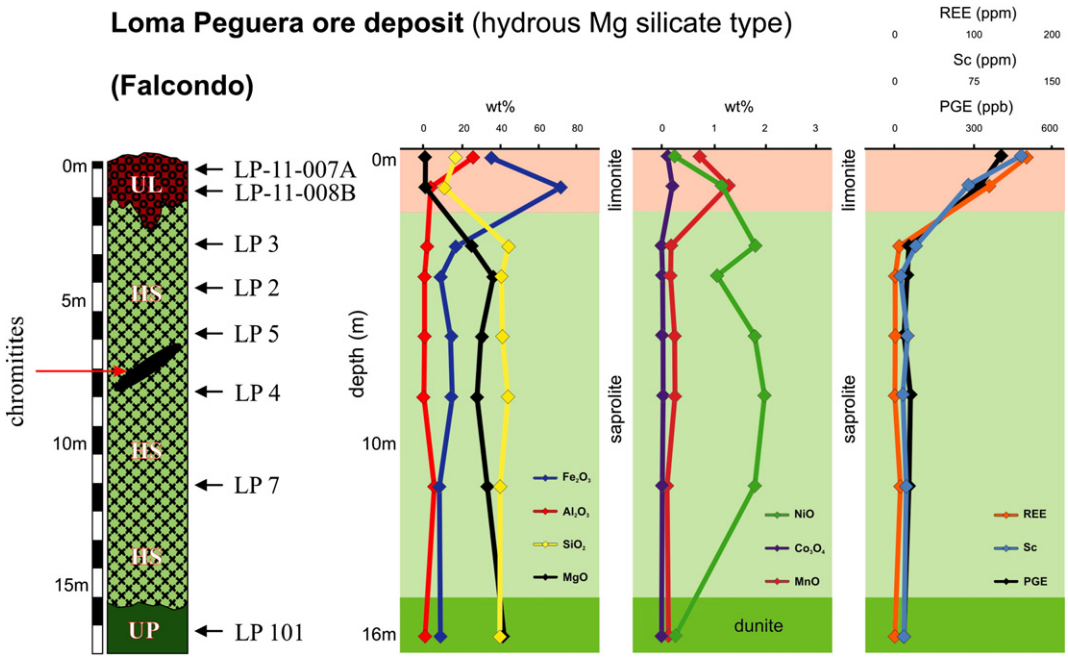

Fig. 7. Ni laterite profile from the Loma Peguera ore deposit (Falcondo) showing location of samples with major, relevant minor elements and CM contents.

3.2. Whole rock geochemical analyses

Major, minor and trace elements of weathering samples from Moa Bay were determined at the Actlabs Laboratories (Ontario, Canada) by X-ray fluorescence (XRF) and ICP mass spectrometry (ICP-MS), respectively (Table 1). Weathering samples from Falcondo were analysed by the same methods at the University of Granada (Table 1) (see Lázaro et al., 2013 for details on the applied analytical techniques). Hard rock samples of unweathered peridotite were analysed for major, minor and trace elements at the ISTEEM (Universite´ Montpellier II, Montpellier, France; see Marchesi et al., 2006 for details on the applied analytical techniques).

PGE contents were obtained at Genalysis Ltd. (Maddington, Western Australia) by ICP-MS (detection limits, 1 ppb for Rh and 2 ppb for Os, Ir, Ru, Pt, and Pd) after nickel sulphide fire assay collection, following the method described by Chan and Finch (2001) (Table 1).

3.3. Mass balance calculations

Mass balance calculations were achieved by using the open source software GCDkit 3.00 (www.gcdkit.org) and its implementation for ISOCON mass balance calculations after Grant (1986, 2005).

3.4. X-ray diffraction analyses

X-ray powder diffraction measurements were performed on homogenized sample aliquots in a Bragg–Brentano θ/2θ Siemens D-500 diffractometer (radius = 215.5 mm) with Cu Kα radiation, selected by means of a secondary graphite monochromator. The divergence and receiving slits were of 1° and 0.15° respectively. The starting and the final 2θ angles were 4° and 80° respectively. The step size was 0.03° 2θ and the measuring time of 18 s per step. Mineral identification was made using the X´Pert HighScore software (Degen et al., 2014).

3.5. Hydroseparation

Heavy mineral concentrates included in polished monolayers were obtained at the hydroseparation (HS) laboratory at the University of Barcelona (http://www.hslab-barcelona.com/) by applying the computer-controlled hydroseparation device CNT HS 11 (Rudashevsky et al., 2001; Rudashevsky and Rudashevsky, 2006, 2007; and see http://www.cnt-mc.ru/), following the proposed methodology for soft rocks by Aiglsperger et al. (2015).

3.6. Scanning electron microscopy and electron microprobe analyses

Thin sections, in situ polished sections and heavy mineral monolayers were studied with a scanning electron microscope Quanta 200 FEI XTE 325/D8395 and with a field emission scanning electron microscope Jeol JSM-7100 at the Serveis Científics i Tecnològics, University of Barcelona, Spain. At the same institution one PGE grain with complex textures was investigated by element-distribution maps using a JEOL JXA-8230 electron microprobe with an accelerating voltage of 20 kV and a beam current of 128.8 nA. Maps were collected by beam scanning with dwell times of 60 ms/pixel. For each element, the background map was subtracted from the corresponding peak map.

3.7. Laser ablation-inductively coupled plasma-mass spectrometry (LA ICP-MS)

An Element 2 high resolution mass spectrometer coupled with a 213-nm NdYAG UP-213 laser ablation system placed at the Institute of Geology, Prague (The Czech Academy of Science) was used to acquire the trace element data. The following isotopes were measured at the low mass resolution mode ($m/\Delta m = 300$): ^{45}Sc, ^{57}Fe, ^{89}Y, ^{90}Zr, ^{99}Ru, ^{101}Ru, ^{103}Rh, ^{104}Pd, ^{108}Pd, ^{110}Pd, ^{111}Cd, ^{139}La, ^{140}Ce, ^{141}Pr, ^{146}Nd, ^{147}Sm, ^{151}Eu, ^{159}Tb, ^{160}Gd, ^{161}Dy, ^{165}Ho, ^{166}Er, ^{169}Tm, ^{172}Yb, ^{175}Lu, ^{185}Re, ^{189}Os, ^{193}Ir and ^{195}Pt.

Trace elements, REE and PGE were calibrated against the synthetic silicate standard glass NIST SRM 610 (Jochum et al., 2011). The isotope ^{57}Fe was used as the internal standard. All standards were run before and after each set of 10 unknowns.

Polished resin blocks were used for in situ laser ablation analyses. Both external standards and measured samples were analysed at identical conditions: laser ablation repetition rate of 10 Hz, the laser fluence of 5–7 J/cm^2 and 55 μm beam spot. Data for the gas blank were acquired for 35 s followed by 35 s of laser ablation signal. The washout time was 120 s between measuring of individual laser spots. Samples were ablated in an in-house small volume ablation cell, a construction which was

inspired by conception of Kooijman et al. (2012). The ablated material was transported by a high purity He gas from the laser ablation cell at a flow rate of 0.4–0.6 l/min.

The time-resolved signal data of spot analyses were processed using the Glitter software (van Achterbergh et al., 2001). The precision of the laser ablation analyses (as relative 1 sigma error — RSD) ranges between 5 and 15% for most of the detected elements.

4. Results

4.1. Geochemistry

4.1.1. Moa Bay

Fig. 5 shows the general geochemical trend within the oxide type laterite from Moa Bay with respect to the distribution of major elements (Fe, Al, Si and Mg), relevant minor elements (Ni, Co and Mn) and CM (REE = La + Ce + Nd + Sm + Eu + Tb + Yb + Lu, Sc and PGE = Os, Ir, Ru, Rh, Pt, Pd). Mg and Si are main components in the saprolite (~40 wt.%) but extremely depleted in the limonite where Fe and Al prevail (~65 wt.% and ~10 wt.% respectively) (Fig. 5). Ni shows significant enrichment (2.3 wt.%) at the transition zone between saprolite (~0.5 wt.%) and lower limonite (~1 wt.%) (Fig. 5). Co enrichment up to 0.65 wt.% is observed within zones of significant Mn oxide(s) accumulation (up to 4.2 wt.% MnO) (Fig. 5).

Critical elements are enriched in the limonite, especially within zones with elevated concentrations of Mn oxide(s) as well as towards the surface (Fig. 5). Total REE concentrations are low in the unweathered harzburgite (~0.1 ppm) and vary from 1 to 3 ppm in the saprolite and from 15 to 68 ppm in the limonite (Table 1). REE chondrite normalized patterns for weathering products show in general rather flat trends with slight negative slopes from La–Eu and slight positive slopes from Ho–Lu (Fig. 8a). The parent rock (harzburgite) shows a pronounced positive slope from Tb–Lu (Fig. 8a). Cerium anomalies are observed in the saprolite (negative) and in the limonite (positive and negative) (Fig. 8a). Scandium and PGE contents of the unweathered harzburgites were not analysed in Marchesi et al. (2006). However, Sc contents range from 8 to 17 ppm in the saprolite and from 70 to 98 ppm in the limonite whereas PGE concentrations vary from 27 to 61 ppb in the saprolite and from 109 to 239 ppb in the limonite (Table 1, Fig. 5). In general saprolite and limonite samples have similar flat PGE chondrite normalized patterns with slight peaks of Ru and Pd as previously observed in Ni laterites from Falcondo (Fig. 9) (Aiglsperger et al., 2015). However, one sample from the Mn oxide(s) rich limonite horizon (i.e. Mn 3) shows a clear positive Pt anomaly and duricrust samples (i.e. 92401 and Mn 17) have slightly negative patterns from Pt to Pd (Fig. 9).

4.1.2. Falcondo

Major elements in Ni laterites from Loma Caribe and Loma Peguera (Figs. 6, 7, respectively) follow the general trend for Ni laterites with characteristic enrichment of Fe + Al towards the surface and Si + Mg depletion within the limonite. Close to the surface Al shows a significant peak of up to ~30 wt.% in both Ni laterite locations, whereas Fe decreases from ~60 to ~40 wt.% (Loma Caribe) and from ~70 to ~35 wt.% (Loma Peguera) (Table 1, Figs. 6, 7). Within the Ni laterite profile of Loma Caribe two Mn rich levels are observed: one at the transition zone between saprolite and limonite (8.4 wt.%) and one in the lower part of the upper limonite (2.2 wt.%) (Fig. 6). Co enrichment (1.68 wt.% at the transition zone and 0.6 wt.% in the upper limonite) correlates with Mn enrichment.

CM are constantly enriched from parent rock to limonite: the parent rock from Loma Caribe contains 0.6 ppm REE, 11 ppm Sc and 30 ppb PGE, slightly enriched saprolite contains 0.9 to 1.6 ppm REE, ~14 ppm Sc and ~50 ppb PGE whereas the limonite concentrates 37 to 335 ppm REE, 41 to 123 ppm Sc and 35 to 264 ppb PGE (Table 1, Fig. 6). Highest REE and Sc contents are observed within a clay minerals rich layer in the lower part of the upper limonite whereas the highest PGE contents occur at the top of the profile (Fig. 6). In general REE chondrite normalized patterns of weathering products from Loma Caribe are slightly negative from La–Eu and flat from Eu–Lu (Fig. 8b). Ce positive anomalies in saprolite and limonite samples as well as a clear Ce negative anomaly in one clay minerals rich limonite sample (i.e. LC 5) are evident (Fig. 8b).

The Ni laterite profile at Loma Peguera shows, similar to Loma Caribe, Mn and Co enrichment (1.3 wt.% and 0.2 wt.% respectively) close to the transition zone between saprolite and limonite (Fig. 7). Slight enrichment trends of CM occur from parent rock (0.2 ppm REE, 8 ppm Sc and 36 ppb PGE) to saprolite (0.5 to 6 ppm REE, 5 to 21 ppm Sc and 37 to 62 ppb PGE) whereas a more significant enrichment is observed within the limonite towards the surface: values reach 122 to 171 ppm REE, 70 to 121 ppm Sc and 331 to 412 ppb PGE (Table 1, Fig. 7). Values of up to 640 ppb total PGE were reported from highest levels in the same Ni laterite profile (Aiglsperger et al., 2015). In general, saprolite and limonite exhibit flat REE chondrite normalized patterns in contrast to HREE enriched patterns in the parent rock (dunite) (Fig. 8c). A distinctive Eu positive peak is observed in one sample from the central part of the saprolite (LP 5) as well as pronounced positive and negative Ce trends in the highest limonite sample and underlying limonite sample, respectively (Fig. 8c).

4.2. Isocon analysis and element transfer

The isocon method described by Grant (1986) was applied to evaluate the potential redistribution of major, minor and critical elements from parent rock to surface during serpentinisation and lateritization. This method is a graphical approach to the mass balance equation used by Gresens (1967) and was previously used to determine element mobility in various rock types (e.g. Meyer et al., 2002; Medaris et al., 2003; Tsikouras et al., 2009; Frost et al., 2013; Liivamägi et al., 2014; Trincal et al., 2014; Chu et al., 2015).

Choosing immobile elements for mass balance calculations is a challenging task. However, sample/bedrock comparisons of all measured elements suggest that Ti and Zr are relatively immobile within investigated Ni laterites. In the case of the Ni laterite from Moa Bay only Ti could be used for mass balance calculations as the Zr content in the protolith is very low (55 ppb; Marchesi et al., 2006) and Zr concentrations for subsequent saprolite samples are below detection limits (Table 1). Because Sc and PGE were not analysed in the average harzburgite of Moa Bay (Marchesi et al., 2006), concentrations of these elements in the less weathered sample (Mn 20) were taken for mass balance calculations.

4.2.1. Moa Bay

Fig. 10 shows gains and losses in wt.%, ppm or ppb relative to the parent rock. During the weathering of peridotite Mg and Si are continuously lost and up to −20% (−7.46 wt.%) of the initial Mg content and approximately −10% (−3.82 wt.%) of the initial Si content have been removed in the higher levels of the saprolite. In contrast Fe gain doubles (+8.36 wt.%) and Al reaches gains of up to +190% (+1.2 wt.%) relative to unweathered peridotite. Within the investigated limonite of Moa Bay mass balance calculations reveal that nearly all Mg (−38 wt.%) and Si (−38 wt.%) are lost. Fe and Al show gains in the lower limonite (up to +6.5 wt.%, +84% and +1.2 wt.%, +188% respectively) but are subsequently lost within the duricrust on top of the profile (−6.5 wt.%, −84% and −0.3 wt.%, −54% respectively).

With respect to the mass balance of Ni, Co and CM, Fig. 10 indicates important gains of Ni (up to +15,000 ppm) together with Co (up to +145 ppm), Sc (up to +9 ppm), LREE (up to +3 ppm) as well as PGE (up to +34 ppb) in the saprolite. HREE were all below detection limit in samples in the saprolite and could not be balanced (Table 1). Within the lower limonite Ni reaches gains of up to +700 ppm (+31%), Co up to +700 ppm (+721%), Sc between +6 ppm (+65%) and +12 ppm (+130%), LREE up to +11 ppm (1000 fold), HREE up to +3 ppm (6 fold) and PGE up to 14 ppb (+53%). In contrast, duricrust

Table 1
Concentrations of relevant major and minor elements (in wt.%) as well as trace elements (in ppm or ppb) in parent rocks and weathering products of Ni laterite profiles from the Punta Gorda ore deposit (Moa Bay), Loma Caribe ore deposit (Falcondo) and Loma Peguera ore deposit (Falcondo). DC (duricrust); UL (upper limonite); LL (lower limonite); SS (soft saprolite); HS (hard saprolite); SP (saprolite); UP (unweathered peridotite); UMIA (ultramafic index of alteration; see text for explanation).
Values of the parent rock from Punta Gorda (*av. Hzb.*) are taken from Marchesi et al. (2006).

	Punta Gorda ore deposit, oxide type (Moa Bay)										Loma Caribe ore deposit, hydrous Mg silicate type (Falcondo)		
	92401	Mn 17	92402	92405	92407	Mn 3	Mn 5	92424	Mn 20	av. Hzb.	LC-11-001	LC-1	LC-2
	DC + UL	DC + UL	LL	LL	LL	LL	SP	SP	SP	UP	DC + UL	UL	UL
wt.%													
SiO_2	2.72	2.69	4.35	3.18	3.92	3.58	35.17	41.36	39.43	38.59	6.46	14.60	6.64
Al_2O_3	14.52	15.00	9.59	9.16	8.26	7.98	1.84	1.04	0.94	0.64	31.82	14.16	9.72
Fe_2O_3	68.03	65.81	66.75	71.83	69.13	68.66	16.17	9.22	9.28	7.81	40.10	55.97	65.55
MnO	1.07	0.38	0.83	1.02	1.60	4.24	0.18	0.12	0.12	0.11	0.26	0.38	2.24
MgO	0.56	0.72	1.73	0.28	1.19	0.49	30.81	39.16	35.69	38.27	0.11	1.05	0.57
CaO	0.03	0.04	0.03	0.04	0.05	0.05	0.03	0.27	0.06	0.32	0.02	0.06	0.01
Na_2O	0.07	0.11	0.12	0.13	0.17	0.15	0.07	0.05	0.06	<dl	0.06	0.08	<dl
K_2O	0.08	0.06	0.06	0.07	0.09	0.13	0.03	0.03	0.03	<dl	0.04	0.10	<dl
TiO_2	0.48	0.51	0.06	0.08	0.05	0.06	0.01	0.01	0.01	0.01	3.33	0.78	0.26
P_2O_5	0.05	0.03	0.02	0.02	0.01	0.02	0.01	0.01	0.01	n.a.	0.07	0.05	0.02
Cr_2O_3	2.40	4.05	3.34	2.78	4.13	2.13	0.81	0.32	0.34	n.a.	0.49	1.70	1.82
Co_3O_4	0.03	0.01	0.16	0.14	0.25	0.65	0.03	0.02	0.02	n.a.	0.02	0.05	0.55
NiO	0.65	1.38	1.69	1.75	1.89	1.06	2.28	0.40	0.52	n.a.	0.63	0.89	1.42
LOI	8.90	10.55	10.50	9.13	8.07	10.46	13.09	8.74	13.91	14.29	16.34	9.47	9.54
ppm													
Rb	3.0	0.4	3.0	4.0	4.0	<dl	<dl	<dl	<dl	0.0	<dl	6.0	<dl
Cs	0.6	0.1	<dl	<dl	<dl	<dl	<dl	<dl	<dl	0.4	<dl	1.2	<dl
Be	<dl	0.5	<dl	<dl	<dl	<dl	<dl	<dl	<dl	0.0	<dl	<dl	1.4
Sr	16.0	6.9	3.0	3.0	4.0	74.0	4.0	<dl	3.0	0.7	5.0	17.0	<dl
Ba	48.0	6.3	25.0	26.0	122.0	1269.0	17.0	5.0	12.0	n.a.	<dl	22.0	20.4
Sc	70.0	72.0	85.0	98.0	86.0	85.0	17.0	12.0	8.0	n.a.	87.0	58.0	55.6
V	387.0	195.2	339.0	361.0	364.0	362.0	65.0	45.0	33.0	38.2	822.0	306.0	202.9
Cr	16,438.4	27,760.8	22,876.7	19,041.1	28,287.7	14,589.0	5670.0	2150.0	2230.0	2669.2	3260.0	6986.2	12,496.7
Co	203.0	106.0	1205.9	949.0	1838.2	4750.0	241.0	90.0	112.0	96.4	100.0	309.0	4008.1
Ni	4610.0	10,851.8	13,312.4	13,776.0	14,844.8	8322.2	17,878.2	2620.0	3610.0	2265.4	4600.0	6670.0	11,189.8
Cu	90.0	140.8	150.0	150.0	170.0	190.0	30.0	<dl	20.0	n.a.	80.0	60.0	75.4
Zn	230.0	129.8	490.0	280.0	520.0	460.0	110.0	<dl	50.0	n.a.	<dl	230.0	262.6
Ga	17.0	9.7	10.0	10.0	10.0	9.0	2.0	1.0	1.0	n.a.	33.0	20.0	12.1
Y	2.0	3.3	<dl	<dl	6.0	5.0	<dl	<dl	<dl	n.a.	6.0	3.0	7.8
Nb	8.0	5.3	<dl	<dl	<dl	<dl	<dl	<dl	<dl	0.0	1.0	11.0	<dl
Zr	85.0	36.0	23.0	32.0	29.0	7.0	5.0	<dl	<dl	0.1	114.0	115.0	24.3
Hf	1.8	1.8	<dl	<dl	<dl	<dl	<dl	<dl	<dl	0.0	3.2	3.0	0.4
Pb	12.0	5.1	<dl	<dl	<dl	7.0	<dl	<dl	<dl	n.a.	<dl	11.0	<dl
U	2.3	2.0	0.2	0.3	0.1	0.5	<dl	<dl	<dl	0.0	0.4	2.3	<dl
Th	7.3	3.3	0.2	0.4	0.1	0.5	<dl	<dl	<dl	0.0	0.4	8.8	0.3
La	8.6	3.9	2.6	2.5	11.6	12.5	1.2	2.2	0.5	<dl	8.5	10.7	3.7
Ce	24.8	9.1	6.5	8.1	1.7	34.6	0.4	0.2	0.3	0.0	53.4	24.6	68.3
Pr	1.7	1.0	0.6	0.5	3.7	2.6	0.1	0.2	0.1	<dl	2.0	2.1	1.9
Nd	6.2	3.7	2.8	2.0	16.2	9.3	0.2	0.5	0.2	0.0	8.6	7.4	8.9
Sm	1.2	0.8	0.8	0.5	6.5	1.8	<dl	<dl	<dl	n.a.	2.2	1.4	3.4
Eu	0.2	0.2	0.2	0.1	1.5	0.5	<dl	<dl	<dl	0.0	0.6	0.3	1.1
Gd	1.0	0.7	0.6	0.4	3.8	1.7	<dl	<dl	<dl	0.0	2.1	1.1	2.3
Tb	0.2	0.1	0.1	<dl	0.8	0.3	<dl	<dl	<dl	0.0	0.3	0.2	0.5
Dy	1.0	0.8	0.7	0.4	4.6	1.6	<dl	<dl	<dl	0.0	2.0	1.2	2.7
Ho	0.2	0.2	0.1	<dl	0.8	0.3	<dl	<dl	<dl	0.0	0.4	0.3	0.5
Er	0.7	0.5	0.4	0.3	2.7	0.9	<dl	<dl	<dl	0.0	1.3	0.8	1.5
Tm	0.1	0.1	0.1	<dl	0.6	0.2	<dl	<dl	<dl	0.0	0.2	0.1	0.3
Yb	0.8	0.7	0.5	0.4	5.2	1.1	<dl	<dl	<dl	0.0	1.5	1.0	2.2
Lu	0.1	0.1	0.1	0.1	0.8	0.2	<dl	<dl	<dl	0.0	0.3	0.2	0.3
ppb													
Os	10	4	12	12	19	8	7	4	3	n.a.	27	19	15
Ir	25	18	22	26	27	22	8	6	3	n.a.	30	24	23
Ru	44	32	43	52	48	42	15	12	8	n.a.	58	42	47
Rh	8	7	9	10	11	13	3	3	1	n.a.	12	8	10
Pt	41	34	53	57	53	107	13	14	6	n.a.	66	33	38
Pd	19	14	42	40	49	47	15	16	6	n.a.	71	26	32
Total (wt.%)	99.60	101.35	99.24	99.61	98.81	99.66	100.53	100.74	100.41	100.04	99.75	99.34	98.34
Total REE (ppm)	46.9	22.0	16.0	15.3	60.4	67.5	1.9	3.1	1.1	0.1	83.4	51.4	97.4
Total PGE (ppb)	147	109	181	197	207	239	61	55	27	n.a.	264	152	165
UMIA	91	90	82	90	84	88	8	4	4	3	84	65	80

is characterized by significant loss of Ni (down to −2169 ppm, −96%), Co (down to −94 ppm, −98%), Sc (down to −6.6 ppm, −73%) and PGE (down to −24.9 ppb, −92%), whereas LREE show strong gains (up to +1 ppm, 90 fold). A general observation with respect to the oxide type Ni laterite of Moa Bay is that enrichment trends of Ni, Sc and PGE strongly correlate with the enrichment trend of Fe (Fig. 10).

Loma Caribe ore deposit, hydrous Mg silicate type (Falcondo)						Loma Peguera ore deposit, hydrous Mg silicate type (Falcondo)							
LC-5	LC-6	LC-7	LC-8	LC-9	C-629	LP-11-007 A	LP-11-008 B	LP-3	LP-2	LP-5	LP-4	LP-7	LP-101
UL	LL	LL-SS	HS	HS	UP	DC + UL	UL	HS	HS	HS	HS	HS	UP
9.79	3.82	2.16	41.27	45.67	43.03	17.21	11.15	44.37	40.07	41.19	44.04	39.98	39.84
23.37	9.39	17.67	1.19	1.15	1.76	26.27	3.50	1.86	0.07	0.58	0.26	5.67	0.84
42.59	67.31	50.60	13.24	12.14	8.59	35.71	72.24	16.86	9.41	14.10	14.59	7.80	8.44
0.67	1.36	8.42	0.26	0.25	0.14	0.73	1.28	0.19	0.17	0.23	0.26	0.11	0.13
0.08	0.56	0.01	28.80	28.65	41.05	0.19	1.04	24.72	35.93	30.55	27.43	33.29	41.23
<dl	0.01	0.05	0.26	0.34	1.90	0.01	0.02	0.28	0.03	0.02	0.01	0.13	1.06
<dl	<dl	0.18	0.05	<dl	<dl	<dl	0.08	<dl	<dl	<dl	<dl	<dl	<dl
<dl	<dl	0.03	0.03	<dl	<dl	0.04	0.05	<dl	<dl	<dl	<dl	<dl	<dl
7.86	0.11	0.34	0.02	0.01	0.06	1.31	0.03	0.01	0.01	0.06	0.01	0.33	0.03
0.27	0.04	0.04	0.01	0.01	0.01	0.13	0.03	0.01	0.01	0.01	0.01	0.01	0.01
0.57	2.41	3.18	0.63	0.32	0.38	0.63	3.12	0.40	0.04	0.17	0.08	0.20	0.35
0.09	0.23	1.68	0.03	0.03	0.02	0.11	0.21	0.02	0.02	0.03	0.03	0.01	0.02
0.27	1.87	1.64	2.34	2.31	0.27	0.26	1.14	1.82	1.08	1.80	2.00	1.81	0.27
15.00	11.96	14.30	12.07	10.59	2.78	16.22	5.05	10.21	13.19	12.31	11.68	11.94	7.62
<dl	<dl	<dl	<dl	<dl	<dl	<dl	<dl	<dl	<dl	<dl	<dl	<dl	<dl
<dl	<dl	<dl	<dl	<dl	<dl	<dl	<dl	<dl	<dl	<dl	<dl	<dl	<dl
1.5	<dl	<dl	<dl	<dl	n.a.	2.0	5.0	<dl	<dl	<dl	<dl	<dl	n.a.
17.3	<dl	2.0	2.0	<dl	<dl	<dl	3.0	<dl	<dl	<dl	<dl	<dl	<dl
221.1	21.0	78.0	34.0	20.3	<dl	9.0	48.0	13.8	6.2	7.0	6.8	6.7	<dl
122.7	82.1	41.0	14.0	13.3	10.5	121.0	70.0	21.1	4.9	11.5	6.6	10.6	8.3
<dl	413.9	234.0	54.0	45.3	60.6	445.0	362.0	72.3	13.9	29.5	13.6	65.2	38.6
3894.2	16,492.9	21,780.8	4170.0	2204.5	2596.9	3420.0	21,369.9	2731.4	241.2	1174.5	518.6	1349.1	2426.9
651.7	1724.8	12,352.9	228.0	207.6	137.0	682.0	1536.8	153.5	137.3	204.0	230.3	96.6	151.1
2109.6	14,714.6	12,895.9	18,389.0	18,192.0	2099.6	1780.0	9680.0	14,300.7	8465.1	14,179.0	15,701.5	14,213.6	2094.9
72.3	81.6	650.0	30.0	29.7	<dl	260.0	220.0	35.6	<dl	<dl	<dl	<dl	<dl
185.9	322.4	960.0	<dl	57.5	46.5	110.0	340.0	62.4	36.5	61.8	48.2	49.2	44.0
29.2	14.7	27.0	1.0	1.6	2.1	27.0	7.0	2.1	<dl	1.3	<dl	5.5	1.1
39.2	8.1	15.0	<dl	<dl	<dl	9.5	16.0	3.9	<dl	<dl	<dl	4.0	<dl
5.4	<dl	<dl	<dl	<dl	3.1	4.3	<dl	<dl	<dl	<dl	<dl	<dl	<dl
267.1	6.5	14.0	5.0	6.0	6.1	63.0	<dl	<dl	7.8	7.1	6.8	22.2	5.6
5.0	<dl	0.4	<dl	<dl	4.7	1.8	<dl	<dl	<dl	<dl	<dl	<dl	<dl
<dl	7.6	<dl	<dl	<dl	<dl	15.0	<dl	<dl	<dl	<dl	<dl	<dl	<dl
0.2	0.1	<dl	<dl	<dl	<dl	1.3	<dl	<dl	<dl	<dl	<dl	<dl	<dl
0.4	<dl	<dl	<dl	<dl	<dl	2.3	<dl	<dl	<dl	<dl	<dl	<dl	<dl
99.8	2.0	4.1	0.2	0.2	0.0	4.2	16.1	0.4	0.1	0.1	0.1	0.5	0.0
80.0	23.1	66.4	0.4	0.8	0.0	150.0	0.6	0.5	0.2	0.1	0.2	1.4	0.0
20.3	0.8	2.3	0.1	0.0	0.0	1.2	6.9	0.2	0.0	0.0	0.0	0.2	0.0
74.7	3.9	9.7	0.2	0.2	0.0	5.0	35.4	1.2	0.1	0.1	0.1	0.9	0.0
15.8	1.2	3.6	<dl	0.1	0.0	1.7	17.4	0.4	0.0	0.0	0.0	0.4	0.0
4.8	0.5	1.1	<dl	0.0	0.0	0.5	4.8	0.2	0.0	0.0	0.0	0.1	0.0
12.9	1.2	3.9	<dl	0.1	0.0	2.0	8.1	0.5	0.0	0.0	0.0	0.5	0.0
2.0	0.2	0.8	<dl	0.0	0.0	0.4	1.8	0.1	<dl	<dl	<dl	0.1	0.0
11.7	1.4	5.1	<dl	0.1	0.1	2.2	11.2	0.4	0.0	0.0	0.0	0.6	0.0
2.1	0.3	1.1	<dl	0.0	0.0	0.5	1.9	0.1	<dl	0.0	0.0	0.1	0.0
5.3	0.9	3.2	<dl	0.0	0.1	1.4	5.6	0.2	0.0	0.0	0.0	0.3	0.0
0.7	0.2	0.6	<dl	0.0	0.0	0.2	1.2	0.0	<dl	0.0	<dl	0.1	0.0
4.5	1.3	3.7	<dl	0.1	0.1	1.4	9.7	0.2	0.0	0.1	0.0	0.4	0.0
0.7	0.2	0.6	<dl	0.0	0.0	0.2	1.4	0.0	<dl	0.0	0.0	0.1	0.0
3	20	25	5	6	7	74	46	6	6	4	11	6	4
3	27	24	6	7	4	72	44	7	5	5	12	6	4
5	49	45	10	13	10	143	85	11	13	9	23	13	9
2	11	9	3	3	2	19	14	3	4	4	3	4	2
0	66	39	9	11	5	64	87	10	12	8	6	16	8
22	25	16	11	15	2	41	55	18	8	7	7	11	9
100.55	99.07	100.30	100.20	101.47	99.98	98.81	98.94	100.75	100.02	101.05	100.40	101.27	99.84
335.3	37.3	106.1	0.9	1.6	0.6	170.7	122.1	4.5	0.4	0.5	0.5	5.6	0.1
35	198	158	44	55	30	411.5	331	55	48	37	62	56	36
75	87	93	6	6	4	62	70	8	4	6	6	7	3

4.2.2. Falcondo

In general the saprolite of the Ni laterite profile at Loma Caribe is characterized by gains of major elements: Mg (+9 wt.%), Si (up to +36 wt.%), Fe (up to +13 wt.%) and Al (up to +0.3 wt.%) (Fig. 11). A sudden change is observed at the transition zone between saprolite and limonite when Mg and Si drops down to approximately −40 wt.% with minor gains of

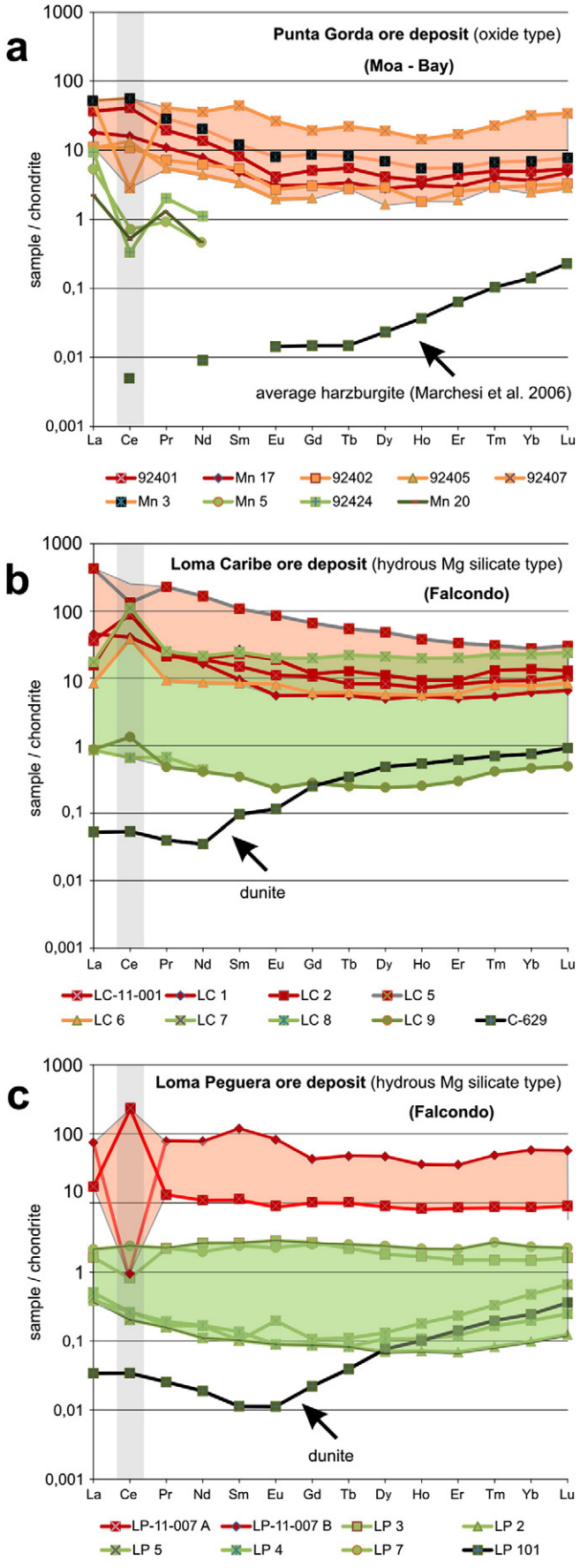

Fe (+4 wt.%) and Al (+3 wt.%). However, Mg and Si remain lost in the subsequent limonite in contrast to gains of Fe (+38 wt.%) and Al (+5 wt.%). Within the limonite a clay-minerals rich layer shows losses of all four major elements (−41 wt.% Mg, −43 wt.% Si, −8 wt.% Fe, −2 wt.% Al). In the lower part of the upper limonite Fe and Al are gained (+7 wt.% and +0.6 wt.%, respectively) whereas at highest levels of the profile significant losses of Fe (down to −7.51 wt.%) and Al (down to −0.9 wt.%) are observed.

In general minor elements as well as CM are gained in the saprolite of Loma Caribe: Ni (up to +30,000 ppm, 14 fold), Co (up to +259 ppm, +189%), Sc (up to +14 ppm, +131%), LREE (up to +2 ppm, 17 fold) and PGE (up to +66 ppb, +219%). In contrast HREE are either lost or measurements of HREE were below detection limit and therefore unsuitable for mass balance calculations (Table 1). However, a gain of HREE (+3 ppm) is observed at the transition zone between saprolite and limonite together with gains of LREE (+23 ppm, 170 fold), Co (+3000 ppm, 22 fold), Ni (+1140 ppm, +54%) and PGE (+10 ppb, +32%). Lower levels of the limonite are generally characterized by gains of Ni (up to +8052 ppm, +384%), Co (up to +1053 ppm, +769%), Sc (up to +46 ppm, +439%), LREE (up to +22 ppm, 168 fold), HREE (up to +3 ppm, +643%) and PGE (up to +107 ppb, +355%). In a clay-minerals rich horizon within the limonite, mass balance calculations reveal a general loss of Ni (−2075 ppm, −99%), Co (−132 ppm, −95%), Sc (−10 ppm, −87%), HREE (−0.2 ppm, −26%) and PGE (−30 ppb, −99%) but a little gain of LREE (+2 ppm, 25 fold). With respect to highest levels of the upper limonite the following elements are lost: Ni (down to −2017 ppm, −94%), Co (down to −135 ppm, −98%), Sc (down to −9 ppm, −78%), HREE (down to −0.3 ppm, −62%) and PGE (down to −25 ppb, −76%). Gains are only observed for LREE (up to +4 ppm, 21 fold).

Gains and losses of major elements in the saprolite of Loma Peguera vary from −37 wt.% to +33 wt.% (Mg), from −35 wt.% to +93 wt.% (Si), from −8 wt.% to +42 wt.% (Fe) and from −1 wt.% to +5 wt.% (Al) (Fig. 12). Within the thin limonite horizon of Loma Peguera Mg and Si are almost entirely lost (approximately −40 wt.% for both elements), whereas Fe (+64 wt.%) and Al (+3 wt.%) are gained in the lower part of the upper limonite. However, at the upper limonite exposed to the surface Fe is lost (−8 wt.%).

Concerning mass balances of Ni, Co and CM in the Loma Peguera Ni laterite profile a continuous gain trend is observed within the saprolite: Ni reaches values of up to +40,000 ppm (+1948%), Co up to +300 ppm (+205%), Sc up to +55 ppm (+663%), LREE up to +10 ppm (100 fold), HREE up to +3 ppm (68 fold) and PGE up to +130 ppb (+358%) relative to underlying dunite. Highest gains in the profile, with exception of Ni (+7600 ppm, +362%), are observed in the lower part of the upper limonite: Co up to +1400 ppm (+917%), Sc up to +62 ppm (+742%), LREE up to +87 ppm (870 fold), HREE up to +55 ppm (1100 fold) and PGE up to +300 ppb (+819%). However, at highest levels of the limonite Ni (−2000 ppm, −97%), Co (−130 ppm, −84%), Sc (−4 ppm, −47%) and PGE (−20 ppb, −58%) are lost, whereas LREE and HREE are slightly gained (approximately +2 ppm for both elements, 30 fold).

Both Ni laterite profiles from the hydrous Mg silicate type at Falcondo reveal rather similar features with respect to mass balance calculations: Ni correlates with Mg and Si, Sc and PGE show a general correlation with Fe (Figs. 11 and 12).

4.3. Profile mineralogy

Fig. 13 gives an overview of the general appearance of alteration products.

Fig. 8. Chondrite normalized REE patterns with highlighted Ce-anomalies and indicated fields of limonite (red) and saprolite (green) of samples from A) Punta Gorda ore deposit (Moa Bay); B) Loma Caribe ore deposit (Falcondo); C) Loma Peguera ore deposit (Falcondo).
Normalization values from Anders and Grevesse (1989).

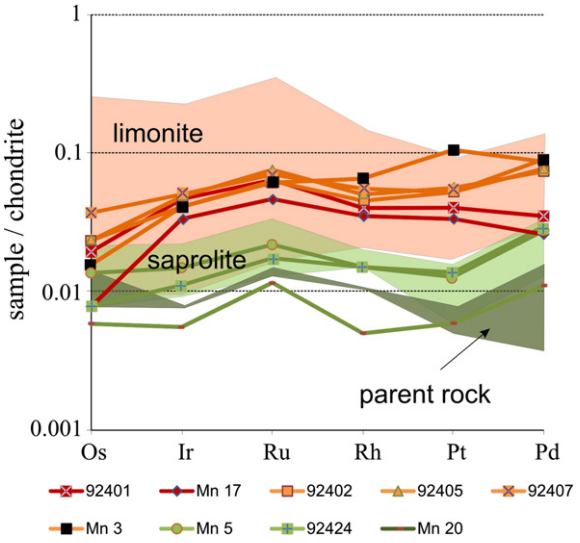

Fig. 9. Chondrite normalized PGE patterns of samples from the Punta Gorda ore deposit (Moa Bay) with indicated fields of limonite, saprolite and parent rock from samples from the Loma Caribe and Loma Peguera ore deposits (Falcondo) (Aiglsperger et al., 2015). Note the positive Pt anomaly in the Mn-oxide rich sample Mn 3. Normalization values from Naldrett and Duke (1980).

4.3.1. Moa Bay

Main minerals found in the serpentinized peridotite are olivine and orthopyroxene (enstatite) crosscut by serpentine minerals (mainly lizardite). Chromian spinel and magnetite occur as minor mineral phases. The saprolite horizon is dominated by lizardite replacing primary olivine grains with goethite and chromian spinel as minor mineral phases. The oxide ore consists mainly of goethite (>50 wt.%) with minor maghemite, hematite and gibbsite. Original textures of the parent rock are not preserved and locally some goethite grains show replacement by hematite. Maghemite is slightly more abundant towards the lowest part of the limonite horizon, whereas hematite is dominant in its upper part. Accumulations of Mn–Co–Ni oxide(s), mainly lithiophorite, Al-rich asbolane and lithiophorite-asbolane intermediate minerals, are present as veins and coatings or concretions along fractures, at certain levels within the lower part of the limonite horizon. Gibbsite is believed to be a less soluble alteration product of plagioclase from the gabbro bodies in the parent rock (Galí et al., 2007). It is more abundant towards the top of the profile (i.e. duricrust). Chromian spinel is an abundant minor mineral phase in the upper limonite. A summary of the observed profile mineralogy from Moa Bay, determined by means of XRD, optical microscopy and SEM, is given in Fig. 14a.

4.3.2. Falcondo

Parent rocks of investigated Ni laterites at Loma Caribe and Loma Peguera are serpentinized dunite and harzburgite, respectively. Olivine and orthopyroxene (enstatite) are major minerals crosscut by abundant serpentine minerals (lizardite). Chromian spinel occurs occasionally as an accessory mineral. The general saprolitic horizon is dominated by Ni-rich lizardite and relicts of olivine and enstatite. Minor clinochlore, goethite, maghemite and/or hematite also occur depending on the individual sample. Chromian spinel and quartz appear only in trace amounts. Major minerals in the limonite horizon are goethite, hematite and gibbsite, whereas lizardite, maghemite and chromian spinel are minor components. Accumulations of Co-bearing Mn oxide(s), mainly heterogenite, Ni-rich asbolane and minor, lithophorite–asbolane intermediate minerals, are found in the transition zone between saprolite and limonite as well as in the central upper limonite. They occur as veinlets, coatings along joints and cracks. In this study observed mineral abundances on the profile scale for Ni laterites from Loma Caribe and Loma Peguera are given in Fig. 14b and c, respectively.

4.4. Critical metal bearing mineral phases

Cerium oxide mineral compounds were detected in heavy mineral concentrates from limonite samples close to the surface at Falcondo. They are always associated with Mn bearing oxide(s) and occur either as rings with diameters of approx. 5 μm (Fig. 15a), as similar sized spheres or as larger aggregates (to 30 μm) of submicron sized flakes (Fig. 15b and c). Cerium oxide in the form of submicrometre to micrometre grains of cerianite with similar shapes has been reported

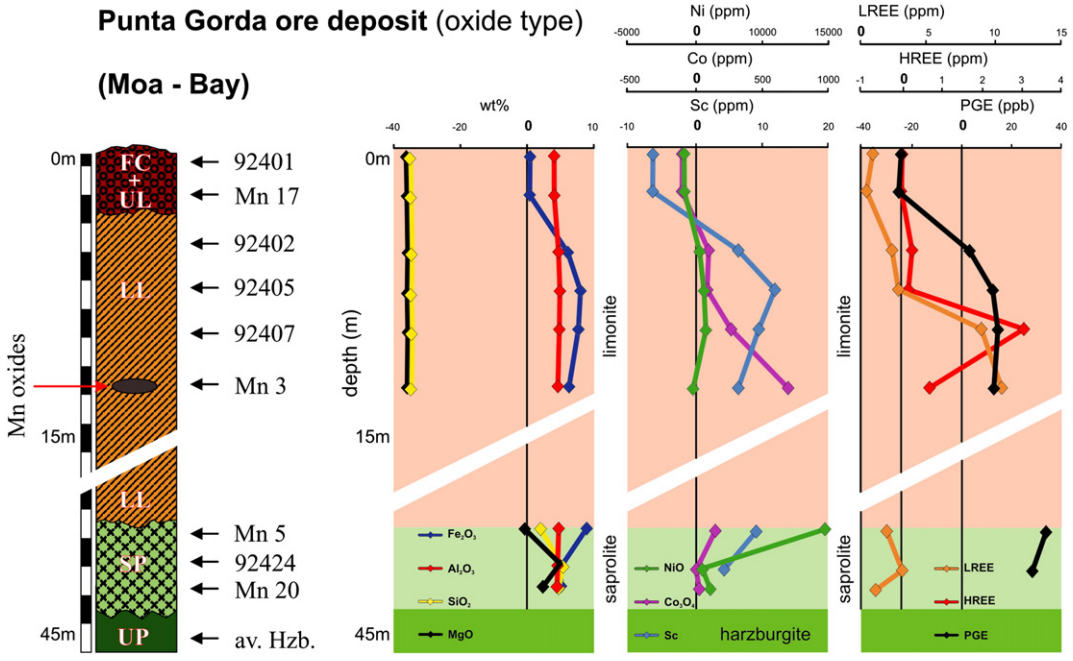

Fig. 10. Isocon analysis of relevant elements in the Ni laterite profile from the Punta Gorda ore deposit (Moa Bay). Vertical lines mark the 0 positions with respect to mass balance calculations.

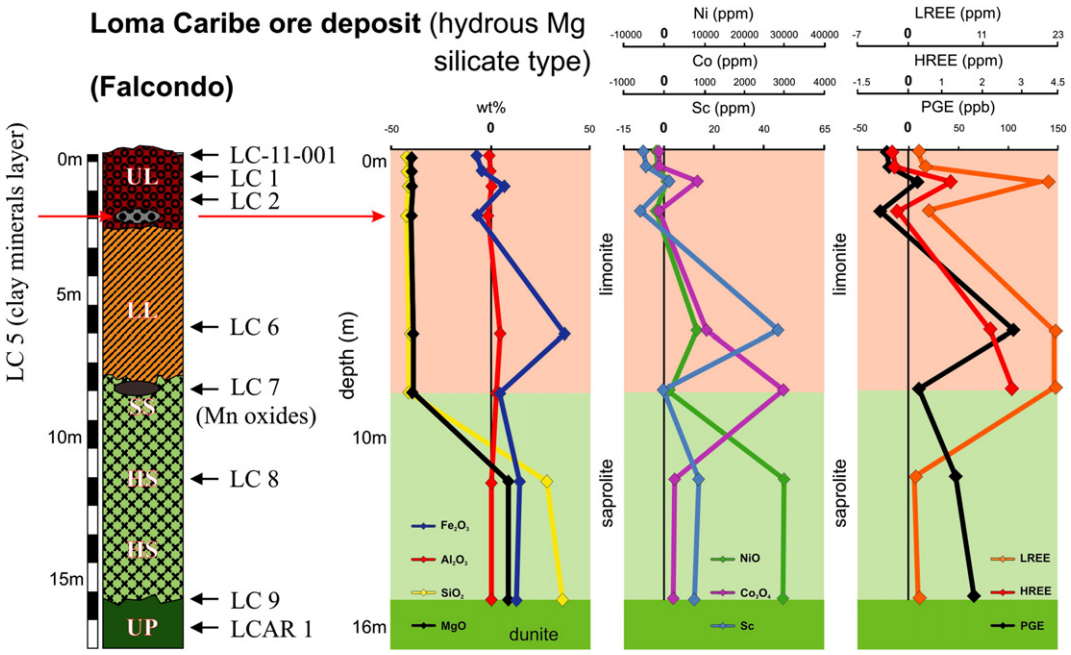

Fig. 11. Isocon analysis of relevant elements in the Ni laterite profile from the Loma Caribe ore deposit (Falcondo). Vertical lines mark the 0 positions with respect to mass balance calculations.

from other lateritic soils around the world (e.g. Braun et al., 1990; Mongelli, 1997; Janots et al., 2015 and reference therein). In the same horizon one small grain (5 μm) of an unidentified La-F mineral phase was found included in secondary Fe oxide(s) (Fig. 15d). REE bearing phosphates were detected in HS concentrates of the upper limonite from Loma Caribe. They are generally associated with secondary Mn oxide(s), one large (~50 μm) free grain with clear crystal faces was also observed (Fig. 15e and f, respectively). Due to the small grain sizes of described REE minerals X-ray diffraction of single crystals for subsequent mineralogical identification was not possible. However, bastnäsite and monazite have been described in Greek laterites by Eliopoulos et al. (2014).

Chromian spinel was observed to contain platinum group minerals (PGM) as small scaled inclusions (<10 μm) and therefore is considered to be the main PGE host at Falcondo (Aiglsperger et al., 2015). However, one Pt–Fe–Ni bearing mineral phase with neoformation features found in secondary Fe oxide(s) from highest levels of the lateritic profile was reported by these authors as well. In general PGM grains found in limonite are small in size (<1 μm to 15 μm) and sometimes occur as very irregular and/or compositionally complex inclusions in secondary Fe oxide(s) (Fig. 16a–c) or awaruite (Fig. 16d). PGM found in the underlying saprolite are different in size and occurrence (Aiglsperger et al., 2015). Examples

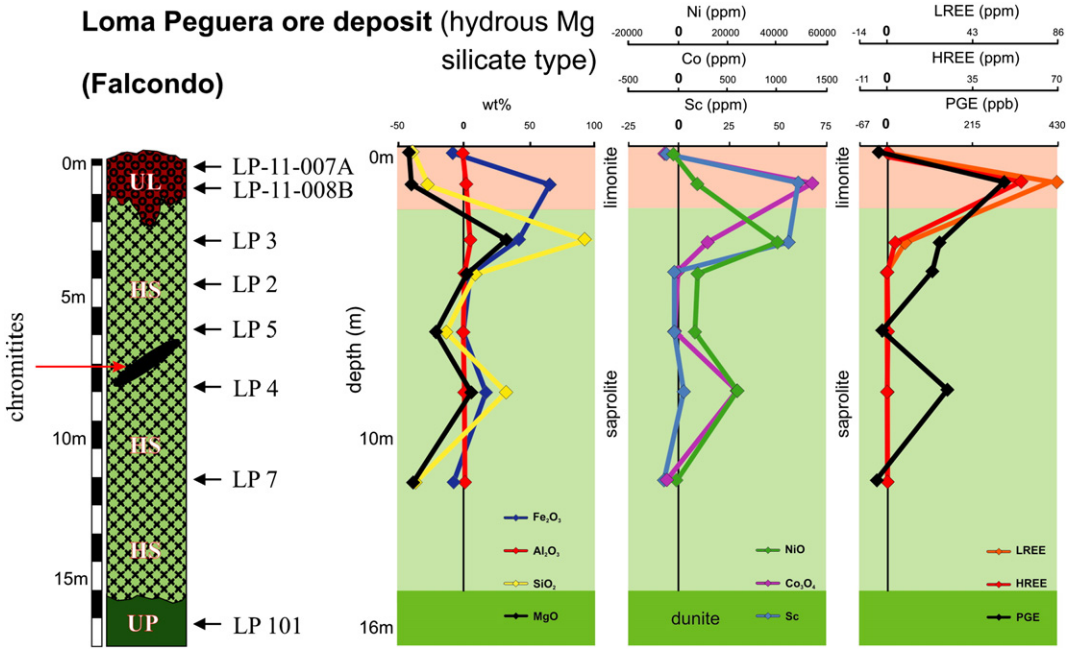

Fig. 12. Isocon analysis of relevant elements in the Ni laterite profile from the Loma Peguera ore deposit (Falcondo). Vertical lines mark the 0 positions with respect to mass balance calculations.

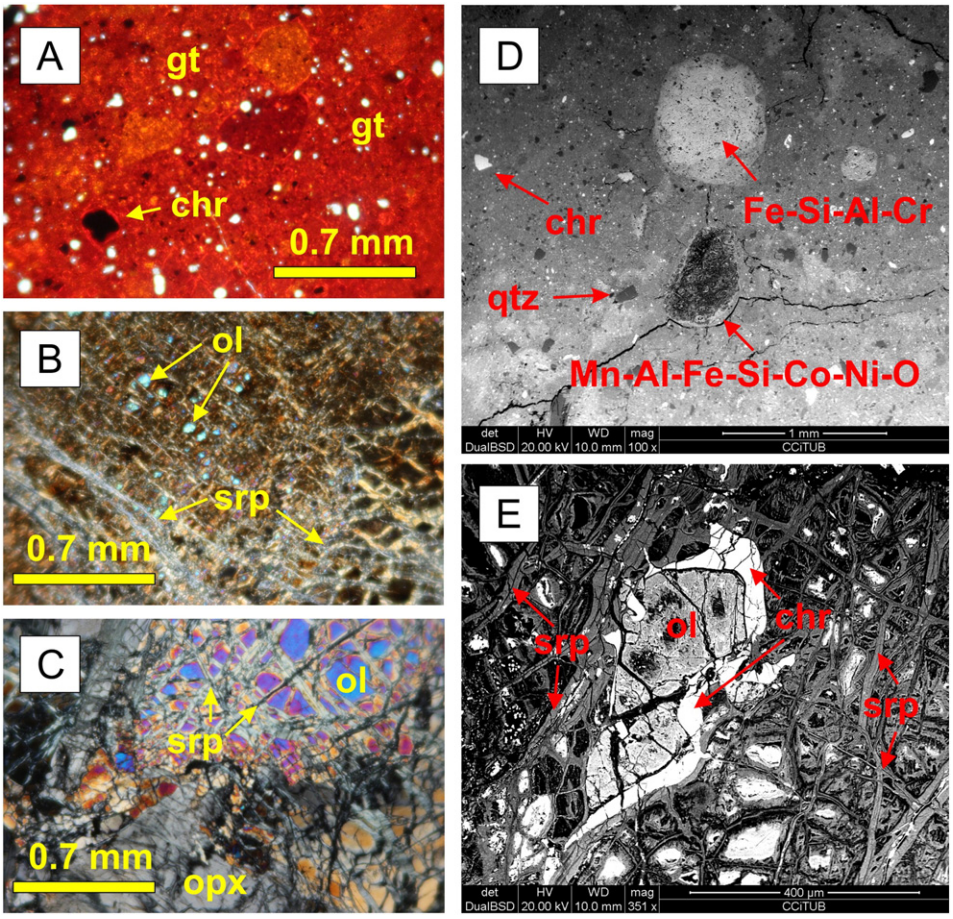

Fig. 13. Cross-polarized photomicrographs (A–C) and BSE images (D and E). A) sample from the limonite horizon mainly consisting of goethite (gt) and minor amounts of chromian spinel (chr); B) sample from the hard saprolite horizon composed of serpentine minerals (srp) with only small remnants of olivine (ol); C) serpentinized peridotite sample with olivine (ol) and orthopyroxene (opx) crosscut by serpentine minerals (srp); D) sample from the limonite horizon containing chromian spinel (chr), quartz (qtz) and unidentified secondary mineral compounds with indicated chemistry; E) sample from the hard saprolite showing a characteristic network of serpentine minerals (srp), olivine (ol) and chromian spinel (chr).

of free grains of altered primary PGM detected in HS concentrates of PGE enriched (~2 ppm total PGE) chromitites from Loma Peguera (Proenza et al., 2007b) are shown in Fig. 16e and f.

Element mapping was applied to one complex PGM found within the upper limonite (Fig. 17). The PGE grain (~15 µm) occurs at the Fe, Ni and Si rich border of a weathered chromian spinel grain and shows aggregate

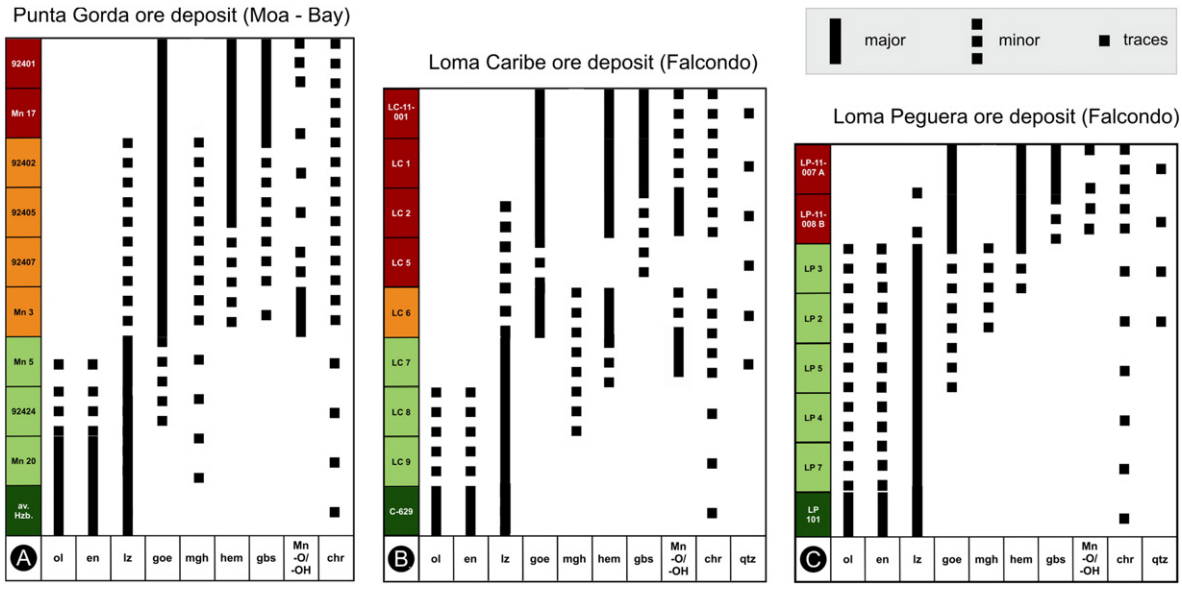

Fig. 14. Summary of identified, characteristic mineral compounds of Ni laterites from A) Punta Gorda ore deposit, B) Loma Caribe ore deposit and C) Loma Peguera ore deposit.

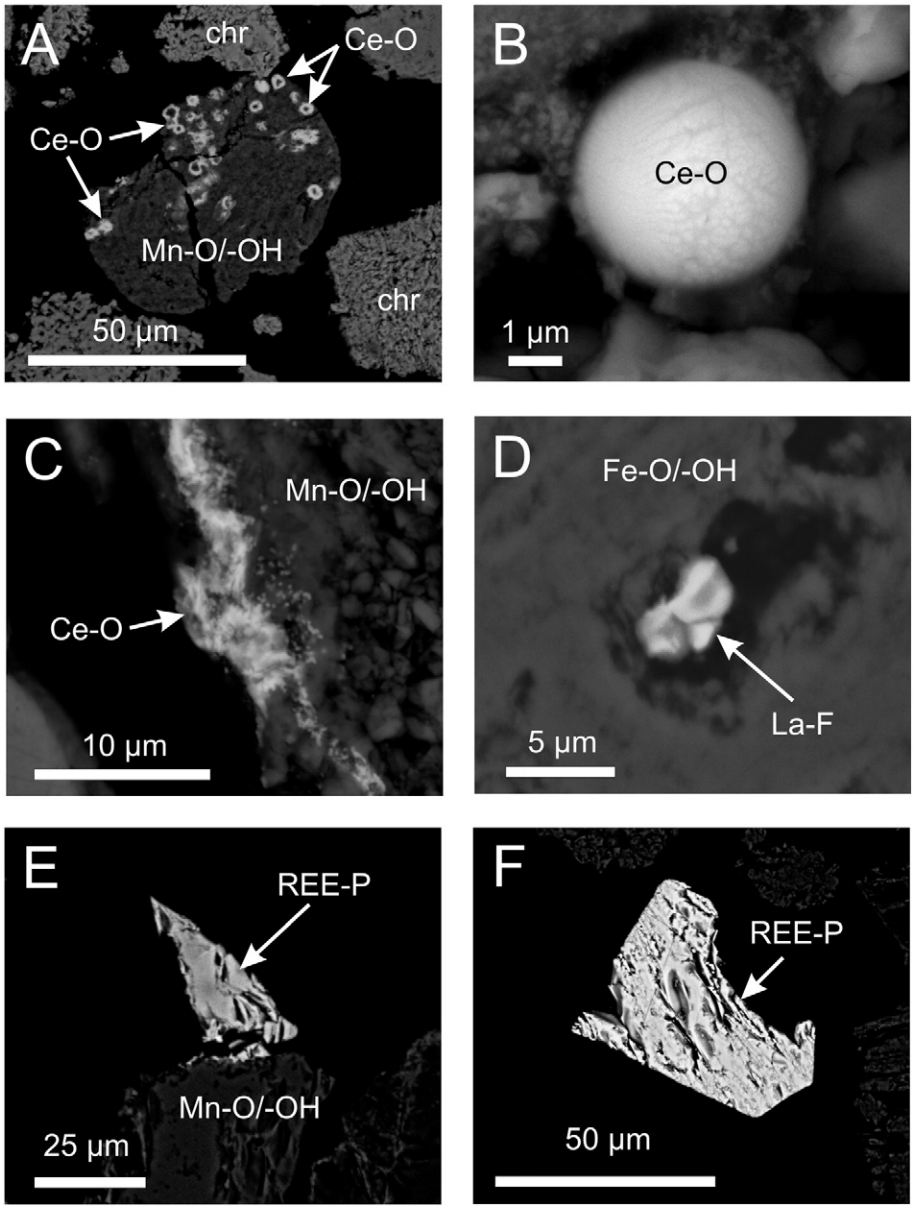

Fig. 15. Selection of BSE images with REE bearing mineral compounds detected in heavy mineral concentrates from the upper limonites. A) Free grain of secondary Mn oxide(s) containing numerous rings of Ce–O; B) close up of one perfectly round Ce–O sphere; C) accumulation of Ce–O nano-flakes at the border of one free Mn oxide(s) grain; D) unidentified La–F grain included in a grain of secondary Fe oxide(s); E) REE–P grain attached to a free grain of Mn oxide(s); F) free crystal of REE–P.

features of submicron particulates. A clear zonation in PGE can be observed at grain scale: Os, Ir and Ru (IPGE) are mainly concentrated in central parts of the grain area, whereas Rh, Pt and Pd (PPGE) are either found in the innermost part (Pt) or at the outside border of the grain (Fig. 17). In addition the element mapping reveals a visual correlation of Ru with As, Rh and Pd with Sb as well as Pt with Ni for zones of highest concentrations. Medium concentrations of Ru in the lower left corner of the image are not detected via back scattered electrons imaging. However, these Ru concentrations correlate visually also with Al, Fe and Si.

Sc vs. Fe_2O_3 discrimination diagrams show two clusters, one for saprolite samples (beneath the Mg discontinuity) and one for limonite and duricrust samples (above the Mg discontinuity), thus suggesting a positive correlation between these elements similar to observations from Ni laterites from New Caledonia (Audet, 2008) (Fig. 18). This indicates that secondary Fe oxide(s) most likely represent the main Sc host in Ni laterites.

LA-ICP-MS analyses on secondary Mn oxide(s) phases from Moa Bay and Falcondo were applied to assess their capacity to host CM and show clear signals for all REE (mainly Ce, La, Pr and Nd), Sc and Pt (Fig. 19).

4.5. The ultramafic index of alteration (UMIA)

In an attempt to quantify and visualize the geochemical changes in Ni laterites developed above ultramafic rocks (e.g. peridotites) an ultramafic index of alteration (UMIA) was defined as:

$$\mathrm{UMIA} = 100 \times \left[\left(Al_2O_3 + Fe_2O_{3(T)}\right)/\left(SiO_2 + MgO + Al_2O_3 + Fe_2O_{3(T)}\right)\right]. \quad (1)$$

This chemical weathering index is based on previous work done by Babechuk et al. (2014) and references therein and considers the dominance of MgO and SiO_2 compared to negligible contents of CaO, Na_2O

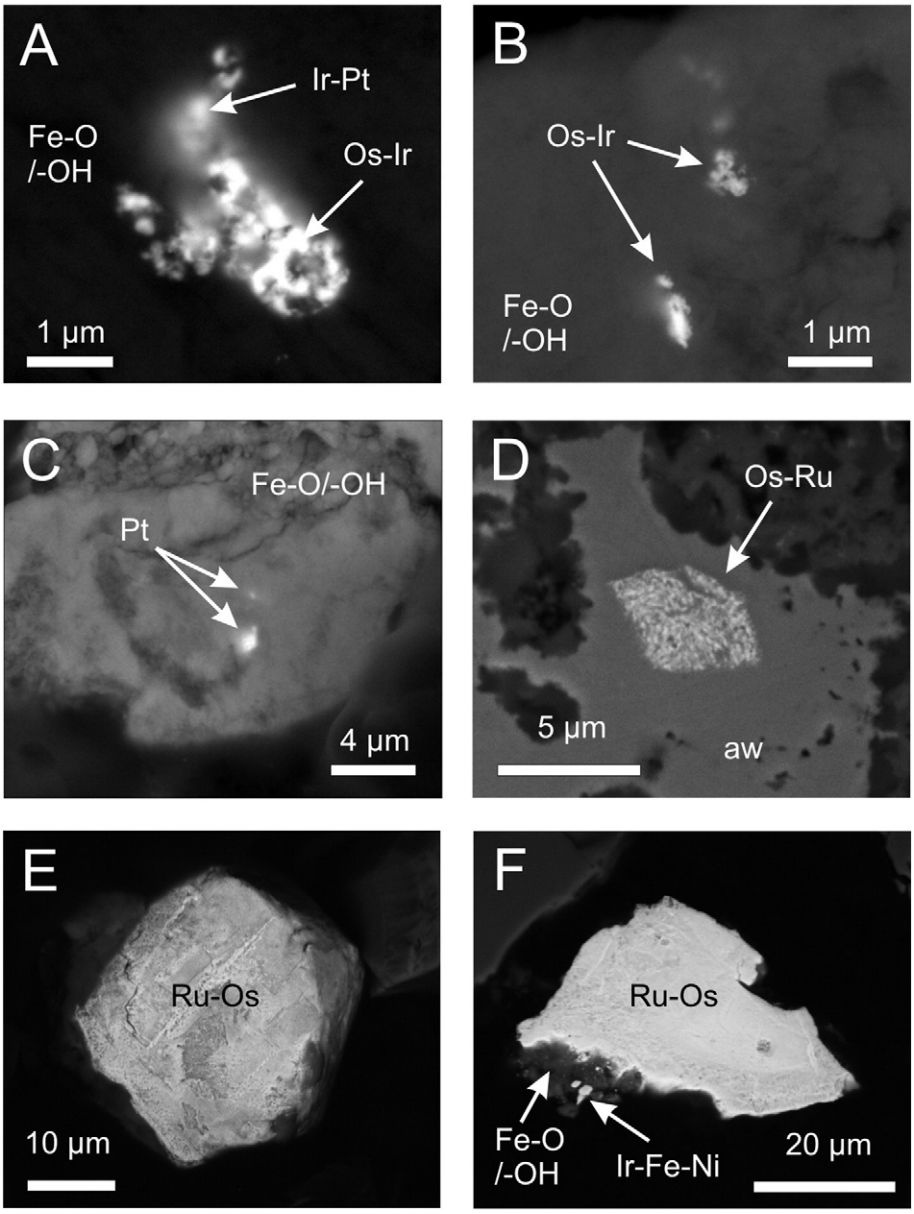

Fig. 16. Selection of BSE images with PGE bearing mineral compounds detected in heavy mineral concentrates from the upper limonites. A) Complex aggregates of nano-particulates consisting of Ir–Pt and Os–Ir included in secondary Fe oxide(s); B) accumulation of Os–Ir bearing nano-particulates at the border of a secondary Fe oxide(s) grain; C) Pt particles at the border of a secondary Fe oxide(s) grain; D) accumulation of Os–Ru bearing nano-particulates at the border of an awaruite (aw) grain; E and F) examples of abundantly occurring free grains of Ru–Os mineral compounds found in chromitite samples from the Loma Peguera ore deposit (Falcondo).

and K_2O in parent rocks as well as the widely observed depletion of MgO and SiO_2 with concomitant enrichment of Fe_2O_3 and Al_2O_3 towards the surface in most Ni laterites. As other chemical weathering indices the UMIA is calculated using molar ratios of the major element oxides by converting wt.% concentrations of whole rock analysis into moles (Duzgoren-Aydin et al., 2002). Unweathered peridotites of this study have UMIA values generally around 3, saprolite samples have UMIA values in the range of 4 to 8 and limonite and duricrust samples reach UMIA values between 60 and >90 (Table 1, Fig. 20).

The proposed UMIA aims to give a general weathering trend for ultramafic rocks. Calculated UMIA values have to be verified by observed mineralogy. For instance locally occurring formation of amorphous silica within highly altered limonite will result in low UMIA values. However, the UMIA can be directly combined with an AF–S–M ternary plot used to illustrate the weathering trend for peridotite samples from investigated Ni laterites (Fig. 20a). Continuous weathering of pyroxene and olivine leads to a loss of Mg and Si whereas redox dependent elements such as Fe are constantly enriched by formation of secondary oxide(s). Trends for either Fe-enrichment or bauxitisation (Al-enrichment) are visualized by an A–F–SM ternary plot (Fig. 20b). Studied Ni laterite samples from Moa Bay are characterized by constantly high Fe/Al ratios, whereas limonite samples from Falcondo are more dispersed and show some tendency to bauxitisation (Fig. 20b).

5. Discussion

5.1. Enrichment and economic significance of critical metals in Ni laterites

Ultramafic rocks exposed to the surface undergo intense chemical and mechanical weathering processes which are mainly controlled by climatic and topographic conditions (Golightly, 1981, 2010; Freyssinet et al., 2005). Supergene processes leach main elements (i.e. Mg and Si) from ferromagnesian minerals in parent rocks whereas other elements (e.g. Ni, Mn, Co) can be enriched up to economic values.

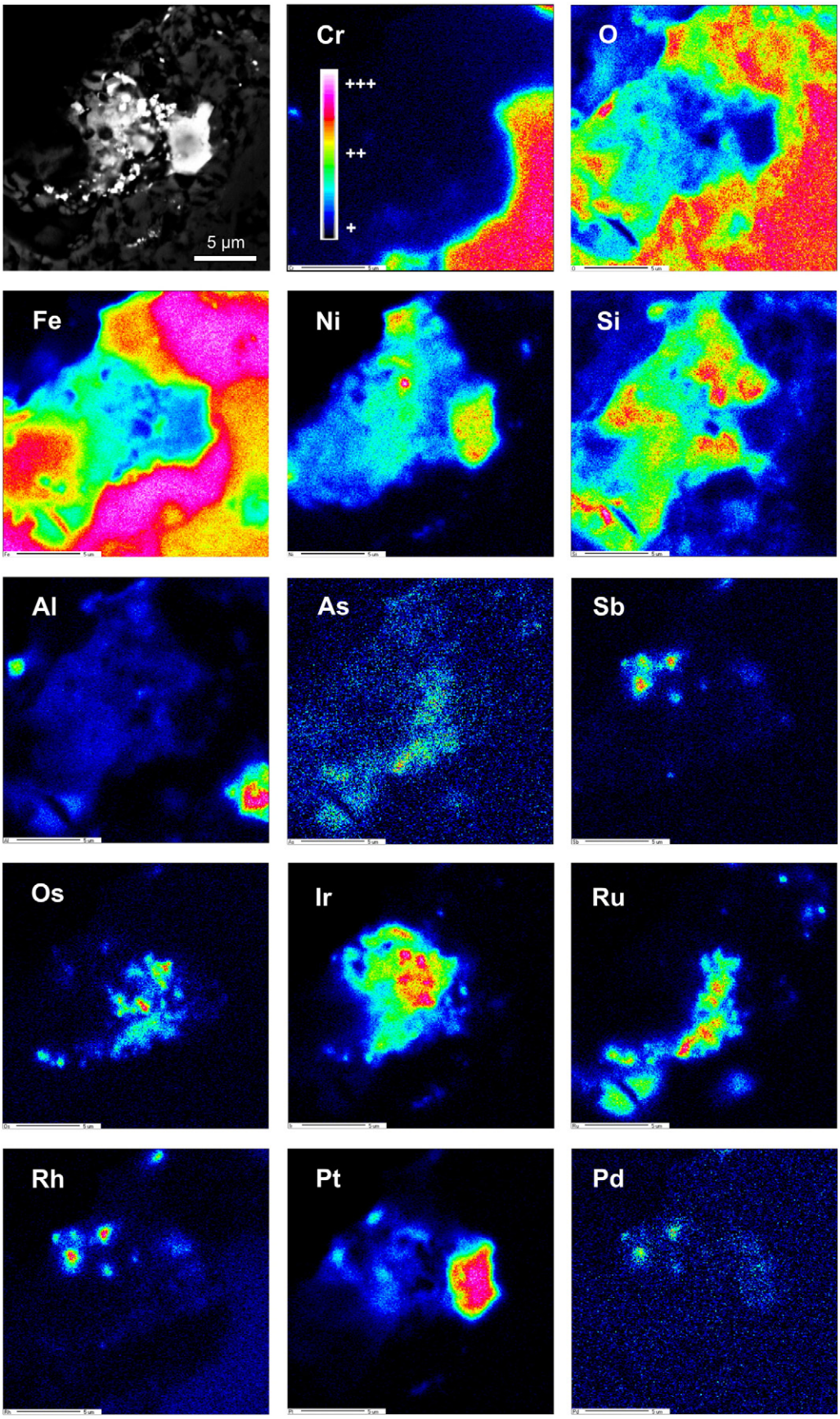

Fig. 17. BSE image and element distribution maps (background corrected) showing the distribution of all PGE and Cr, O, Fe, Ni, Si, Al, As and Sb in a complex PGM grain located at the border of a weathered chromian spinel from the upper limonite of the Loma Caribe ore deposit (Falcondo). Interestingly, Ru contents in the lower left corner of the element distribution map are not observed in the BSE image (dark area).

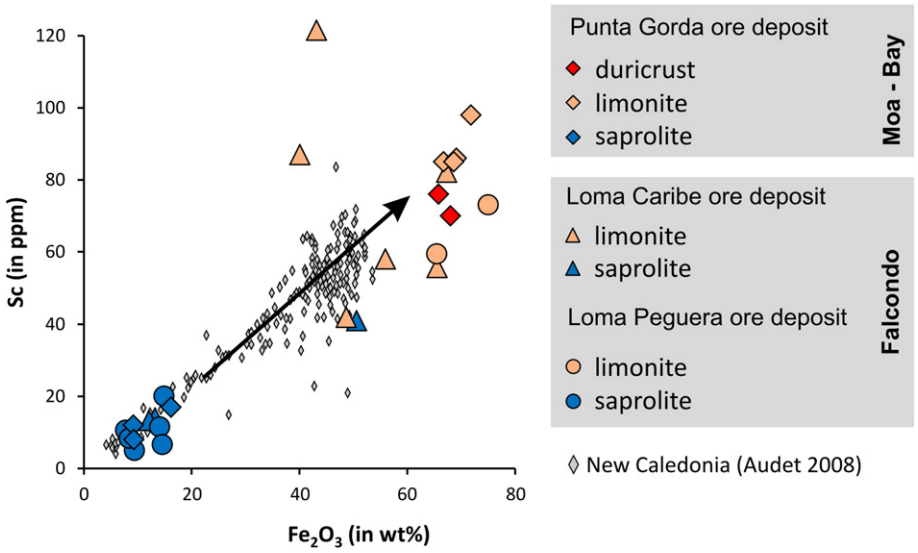

Fig. 18. Sc vs. Fe_2O_3 contents in saprolite, limonite and duricrust showing two clusters indicating a positive correlation as previously observed by Audet (2008) in Ni laterites from New Caledonia.

Redox dependent elements such as Fe as well as rather immobile elements such as Zr and Ti can be residually concentrated towards the surface. Ni laterites are the resulting product and can be classified according to their dominant Ni-bearing mineralogy (Marsh and Anderson, 2011 and references therein). 60% to 70% of the world land-based Ni resources are hosted by Ni laterites (Butt and Cluzel, 2013) and approximately 10% of these Ni resources are located in the northern Caribbean (Dalvi et al., 2004; Lewis et al., 2006a; Nelson et al., 2011). Our results show that large scale Ni laterite deposits can also host relevant amounts of CM.

5.1.1. Rare Earth Elements

It is clear that overall REE contents in investigated Ni laterites are very low when compared with conventional REE ore deposits (Chakhmouradian and Wall, 2012). However, concentrations of up to 335 ppm total REE are reached within clay rich zones in the limonite zone of Loma Caribe (Fig. 6). These values, which always have to be seen in the context of possible additional by-products in operating Ni (+Co) laterite mines, are approximately 10 times less as low grade ion adsorption clay-containing REE deposits. These ores are considered economic under favourable conditions as they are easy to mine and process (Simandl, 2014). Additionally, an important advantage of lateritic REE ores is their very low content of radioactive elements.

The observation of REE minerals as phosphates or as Ce-rings and Ce-accumulations in association with REE enriched secondary Mn oxide(s) reveals that REE are mobilized during the weathering process and can precipitate as newly formed minerals within the limonite (Fig. 15). As a consequence, enrichment peaks of REE are observed at zones with higher MnO accumulations (Figs. 5, 6 and 7). Mass balance calculations of both Ni laterite types reveal that LREE are preferably gained in these horizons compared to minor gains of HREE (Figs. 10, 11 and 12). This observation is supported by LA-ICP-MS analyses on secondary Mn oxide(s) (Fig. 19). However, within the hydrous Mg silicate type Ni laterites at Loma Caribe (Falcondo) the highest concentrations in REE of 335 ppm were found within a clay-minerals rich layer in the limonite (Fig. 6). Mass balance calculations indicate that only LREE are gained (25 fold) in this horizon, which is characterized by a general massive loss of elements relativizing the observed HREE loss of −26% (Fig. 11). Because MnO contents are negligible in this horizon (<0.7 wt.%) a close relationship between clay-minerals and REE (e.g. REE adsorbed on clay-minerals) is suspected.

Within the well-developed duricrust of Moa-Bay (UMIA ~ 90) REE are the only measured elements showing gains in mass balance calculations (Fig. 10). This observation is linked to positive Ce anomalies observed in chondrite normalized patterns of all samples located close to the surface (Fig. 8). Cerium anomalies in lateritic profiles have been interpreted previously by REE leaching in a reducing environment with subsequent oxidation of Ce^{3+} to Ce^{4+} in an oxidizing environment and formation of cerianite (Braun et al., 1990; Janots et al., 2015 and references therein). These authors explained frequently occurring ring structures of cerianite as fillings of pores in a matrix of clay minerals (see Fig. 7c in Braun et al., 1990). However, recent studies on heterogeneous near surface environments (critical zone), which are characterized by complex interactions involving rock, soil, water, air and (micro-)organisms, have shown that heavy-metal mobility in these environments is most likely controlled by biogeochemical processes (e.g. Chorover et al., 2007). In this context the shape of observed cerianite ring structures could alternatively be explained by metal-depositing bacteria as described from experimental studies on bacteria-mineral spatial relationships (Little et al., 1997 and reference therein). The role of microorganisms in the mineralogical and chemical composition of laterite ores has been emphasized by Laskou and Economou-Eliopoulos (2007) and Kalatha and Economou-Eliopoulos (2015) who concluded, due detection of bacteria fossils, that bacterial communities can drive the formation of minerals in these environments. It is widely accepted that microorganisms favour accumulation of lanthanides in biogenic bodies such as Fe–Mn nodules and Fe-ochre (e.g. Vodyanitskii, 2010). Recently, lanthanides even have been proved to be essential for bacterial life in the case of volcanic mudpots (Pol et al., 2014). In addition, metal depositing microorganisms possibly act as subsequent nucleation sites for the precipitation of secondary minerals as likely observed in the case of REE phosphate formation on secondary Mn oxide(s) (Fig. 15e).

5.1.2. Scandium

Although Sc is a high tech element with wide application potential the global scandium consumption is currently estimated in the range of only 10 t (USGS, 2013). This is mainly explained due to high prices in combination with the absence of a reliable long term production for Sc. However, the yearly demand is constantly growing making scandium a worthy exploration target. To date scandium is mainly recovered as by-product from residues, tailings and waste liquors in the production of other metals (Wang et al., 2011). On the other hand, residual

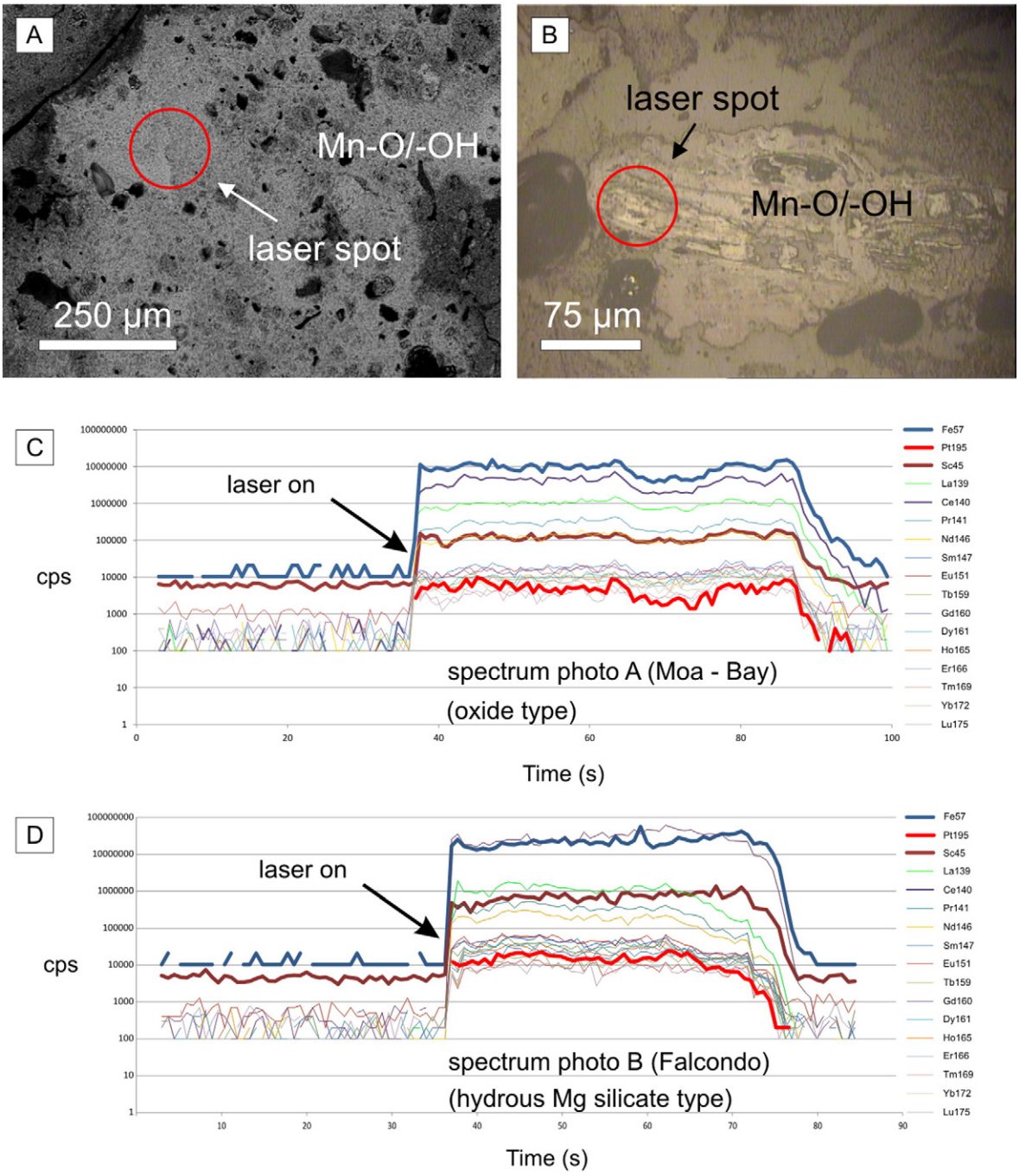

Fig. 19. LA-ICP-MS scans of two spots in secondary Mn oxide(s) from limonite samples from Moa Bay (A and C) and Falcondo (B and D) showing the presence of CM (REE, Sc and Pt) in both cases.

nickel ores in Australia containing average grades of 76 ppm and up to 370 ppm have recently been reported as important scandium resources and industrialized plants for scandium recovery from nickel laterites are expected to produce scandium oxides in large amount (Wang et al., 2011 and reference therein). In fact, highly encouraging extraction results of up to 87% for scandium have been reported very recently from the Owendale laterite ore (Australia) via high pressure acid leach ("HPAL") tests (Platina Resources, 2015).

Sc contents of ~120 ppm, with average contents of approximately 70–80 ppm Sc, were found in the upper limonite in the Ni laterites examined in this study (Figs. 5, 6 and 7). These values are slightly higher than those reported from similar Ni laterites located in New Caledonia (Fig. 18; Audet, 2008). It is believed that Sc is predominantly present in pyroxene minerals of the peridotite as a substitute for ferrous iron. The strong positive correlation with Fe throughout the studied Ni laterite profiles in mass balance calculations (Figs. 10, 11 and 12) indicates that Sc is mainly concentrated in the final weathering products containing ferric iron (Fig. 18). Clear Sc signals in laser ablation ICP-MS analyses on Fe bearing secondary Mn oxide(s) from both Ni laterite types support this assumption (Fig. 19).

5.1.3. Platinum Group Elements

Large oxidized deposits associated with near surface modification of ultramafic rocks have been considered worthy exploration targets for unconventional Pt and Pd deposits (e.g. Wilde et al., 2003). The Owendale platinum–scandium project in New South Wales (Australia), which has estimated mineral resources of 520,000 oz Pt and 9100 t Sc, represents such an exploration target (Platina Resources, 2015). In

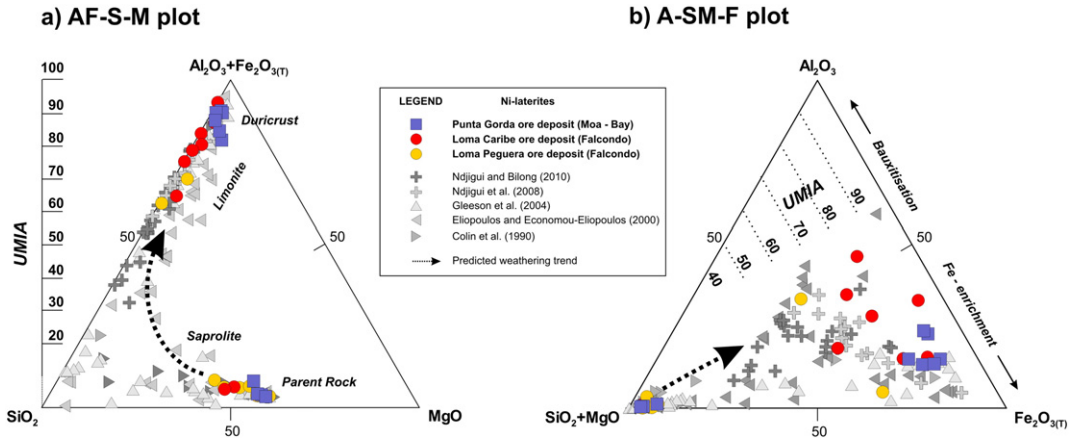

Fig. 20. Molar ternary plots in the Al–Fe–Mg–Si space showing weathering trends of ultramafic rocks and relationships with the in this work defined ultramafic index of alteration (UMIA) with data from the literature and studied samples. A) AF–S–M ternary plot illustrating the general weathering trend of peridotites with initial loss of MgO followed by loss of SiO_2 and concomitant enrichment of Al_2O_3 and Fe_2O_3. B) A–SM–F ternary plot illustrating the weathering trend with respect to Al_2O_3 enrichment (bauxitisation) or Fe_2O_3 enrichment.

general, total PGE concentrations found in Ni laterites around the world are in the range of less than 100 ppb to up to a few hundred ppb (e.g. Augé and Legendre, 1994; Eliopoulos and Economou-Eliopoulos, 2000; Ndjigui and Bilong, 2010). However, lateritic crust with 2 ppm PGE over the Ora Banda Sill, Western Australia, was reported from Gray et al. (1996) as well as more than 4 ppm PGE from Burundi (Maier et al., 2008).

Total PGE concentrations of investigated Ni laterites from the northern Caribbean are systematically enriched in the limonite and reach values of up to a few hundred ppb (Figs. 5, 6 and 7). Mass balance calculations reveal that PGE show similar enrichment trends as Fe, Ni and Sc within both Ni laterite types. PGE are importantly gained within the saprolite as well as within the lower part of the limonite (e.g. up to +358% and +819%, respectively in the case of Loma Peguera) (Figs. 10, 11 and 12). It is believed that PGE are enriched on the profile scale in the residue as PGM inclusions are protected in relatively resistant chromian spinel. However, recent studies also have provided evidence of neoformation processes close to the surface on the local scale (Aiglsperger et al., 2015). The assumption of common PGE redistribution in high levels of tropical Ni laterites is supported by detection of Pt within in-situ formed Mn oxide(s) (Fig. 19). Thus, chondrite normalized PGE patterns of one Mn oxide(s) rich sample (Mn 3) are characterized by a clear positive Pt anomaly (Fig. 9).

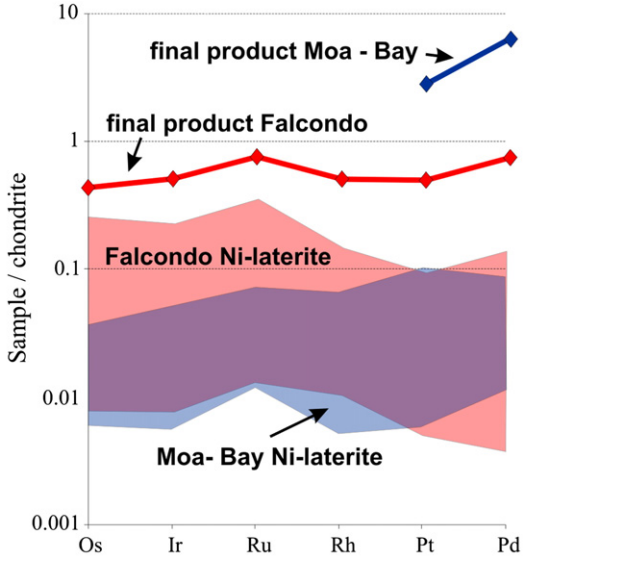

	Os	Ir	Ru	Rh	Pt	Pd	
Falcondo	221	272	529	100	500	403	Σ 2025 ppb
Moa	n.a.	n.a.	n.a.	n.a.	2870	3360	Σ 6230 ppb

Fig. 21. Chondrite normalized PGE patterns and PGE contents of samples from final products from the Moa Bay mining area (values from Lazarenkov et al., 2005) and from the Falcondo mining area (this study) with indicated fields for both Ni laterite mining areas (limonite + saprolite).
Normalization values from Naldrett and Duke (1980).

To assess an economic significance of observed PGE enrichment in Ni laterites the final product of Falcondo (i.e. ferronickel-cone after pyrometallurgical extraction from hydrous Mg silicates found in saprolite) was sent to Genalysis for PGE determination. The results show a PGE concentration of more than 2 ppm total PGE characterized by similar chondrite normalized patterns as for the laterite bulk; however, slightly more positive trends for Ir and Pt are evident (Fig. 21). In addition, Lazarenkov et al. (2005) reported Pt and Pd contents of approximately 3 ppm each from final products from Moa Bay (i.e. sulphide concentrates after high pressure acid leach "HPAL" of oxide(s) (Fig. 21). Considering the higher values measured in final products from Moa Bay, these are probably linked to the exclusive mineral processing of oxidized limonite ores. A similar treatment of limonite ore from Falcondo would likely result in an important increase of total PGE within the final products of Falcondo. Innovative direct extraction technologies such as the carbonyl process recently introduced by Terekhov and Nanthakumar (2013), tested by the authors to be capable to produce 1.7 t PGE from a standard 1,000,000 t limonite Ni ore, as well as ongoing improvements in the metal extraction from oxidized ores by biomining (Johnson and du Plessis, 2015) will probably lead to a more diverse supply chain for these CM in the near future.

6. Concluding remarks

1. CM (REE, Sc, PGE) are concentrated in Ni laterites towards the surface in specific zones: (i) REE in clay minerals rich horizons and within zones composed of secondary Mn oxide(s), (ii) Sc within zones rich in secondary Fe and Mn bearing oxide(s) and (iii) PGE in zones with high concentrations of residual chromian spinel and secondary Fe and Mn bearing oxide(s) at upper levels of the Ni laterite profile.
2. Concentration factors involve (i) residual enrichment by intense weathering, (ii) mobilization of CM during changing Eh and pH conditions with subsequent reprecipitation at favourable geochemical barriers and (iii) interactions between biosphere and limonitic soils at highest levels of the profile with involved neoformation processes.
3. Total contents of CM in investigated Ni laterites are low when compared with conventional ore deposits but are of economic significance as CM should be seen as cost inexpensive by-products during

the Ni (+Co) production. Innovative extraction methods currently under development will boost the significance of Ni laterites as future unconventional high tech metals ore deposits.

Acknowledgements

This research has been financially supported by FEDER Funds, the Spanish projects CGL2009-10924 and CGL2012-36263 and Catalan project 2014-SGR-1661 as well as by a PhD grant and a travel grant to Prague (estancia breve FPI 2013) to TA sponsored by the Ministerio de Economia y Competitividad (Spain). The authors gratefully acknowledge the help and hospitality extended by the staff of Falcondo mine (Falcondo Glencore). Excellent technical support during EPMA sessions by Dr. X. Llovet and during FESEM sessions by Eva Prats at the Serveis Científics i Tecnòlogics (University of Barcelona) is highly appreciated. Louis Cabri and Vladimir Rudashevsky are greatly thanked for their help during installation of the HS-11 laboratory in Barcelona. We want to thank two anonymous reviewers and the editors of OGR for their constructive comments, suggestions and editing.

References

van Achterbergh, E., Ryan, C.G., Jackson, S.E., Griffin, W.L., 2001. Data Reduction Software for LA-ICP-MS. In: Sylvester, P. (Ed.), Laser-ablation-ICPMS in the Earth Sciences: Principles and Applications. Mineralogical Association of Canada, Short Course, pp. 239–243.

Aiglsperger, T., Proenza, J.A., Zaccarini, F., Lewis, J.F., Garuti, G., Labrador, M., Longo, F., 2015. Platinum group minerals (PGM) in the Falcondo Ni laterite deposit, Loma Caribe peridotite (Dominican Republic). Mineral. Deposita 50, 105–123.

Anders, E., Grevesse, N., 1989. Abundances of the elements: meteoritic and solar. Geochim. Cosmochim. Acta 53, 197–214.

Audet, M.A., 2008. Le massif du Koniambo, Nouvelle-Calédonie Formation et obduction d'un complexe ophiolitique du type SSZ. Enrichissement en nickel, cobalt et scandium dans les profils résiduels (PhD thesis (in French), 327 pp.).

Augé, T., Legendre, O., 1994. Platinum-Group Element oxides from the Pirogues ophiolitic mineralization, New Caledonia: origin and significance. Econ. Geol. 89, 1454–1468.

Babechuk, M.G., Widdowson, M., Kamber, B.S., 2014. Quantifying chemical weathering intensity and trace element release from two contrasting basalt profiles, Deccan Traps, India. Chem. Geol. 363, 56–75.

Beaton, D.W., Kryski, K.M., Srivastava, R.M., 2011. 43-101 Technical report on the central Moa nickel laterite operation in Eastern Cuba: Prepared for Sherritt International Corporation. Available at: http://www.sedar.com/GetFile.do?lang=EN&docClass=24&issuerNo=00002460&fileName=/csfsprod/data123/filings/01811517/00000001/z%3A%5Crarcher%5C12941-2081%5CTechRpts%5CMoa.PDF. Accessed 25.03.2015.

Bowin, C.O., 1966. Geology of the central Dominican Republic (a case history of part of an island arc). In: Hess, H. (Ed.), Caribbean Geological Studies. Mem. Geol. Soc. Am. 98, pp. 11–84.

Brand, N.W., Butt, C.R.M., Elias, M., 1998. Nickel laterites: classification and features. AGSO J. Aust. Geol. Geophys. 17, 81–88.

Braun, J., Pagel, M., Muller, J., Bilong, P., Michard, A., Guillet, B., 1990. Cerium anomalies in lateritic profiles. Geochim. Cosmochim. Acta 54, 781–795.

Butt, C.R.M., Cluzel, D., 2013. Nickel laterite ore deposits: weathered serpentinites. Elements 9, 123–128.

Chakhmouradian, A.R., Wall, F., 2012. Rare earth elements: rare earth elements: minerals, mines, magnets (and more). Elements 8, 333–340.

Chan, T.K., Finch, I.J., 2001. Determination of platinum-group elements and gold by inductively coupled plasma mass spectrometry. Australian Platinum Conference, Perth, Western Australia, pp. 1–9.

Chorover, J., Kretzschmar, R., Garcia-Pichel, F., Sparks, D.L., 2007. Soil biogeochemical processes within the critical zone. Elements 3, 321–326.

Chu, H., Chi, G., Bosman, S., Card, C., 2015. Diagenetic and geochemical studies of sandstones from drill core DV10-001 in the Athabasca basin, Canada, and implications for uranium mineralization. J. Geochem. Explor. 148, 206–230.

Dalvi, A.D., Bacon, W.G., Osborne, R.C., 2004. The past and future of nickel laterites. PDAC 2004, International Convention, Prospectors and Developers Association of Canada, March 7–10, Toronto, Ontario, Canada, pp. 1–27.

Degen, T., Sadki, M., Bron, E., König, U., Nénert, G., 2014. The HighScore suite. Powder Diffr. 29, S13–S18.

Draper, G., Gutiérrez, G., Lewis, J.F., 1996. Thrust emplacement of the Hispaniola peridotite belt: orogenic expression of the mid Cretaceous Caribbean arc polarity reversal? Geology 24, 1143–1146.

Duzgoren-Aydin, N.S., Aydin, A., Malpas, J., 2002. Distribution of clay minerals along a weathered pyroclastic profile, Hong Kong. Catena 50, 17–41.

EC (European Commission), 2014. Report on critical raw materials for the EU. Report of the Ad-hoc Working Group in Defining Critical Raw Materials: Brussels, Belgium (Available at http://ec.europa.eu/enterprise/policies/raw-materials/files/docs/crm-report-on-critical-raw-materials_en.pdf. Accessed 25 March 2015).

Economou-Eliopoulos, M., Eliopoulos, D.G., Apostolikas, A., Maglaras, K., 1997. Precious and rare earth element distribution in Ni-laterite deposits Lokris area, Central Greece. In: Papunen, H. (Ed.), Proceedings of the 4th Biennial SGA Meeting, pp. 411–413 (Balkema, Rotterdam, Turku, Finland).

Eliopoulos, D.G., Economou-Eliopoulos, M., 2000. Geochemical and mineralogical characteristics of Fe–Ni- and bauxitic-laterite deposits of Greece. Ore Geol. Rev. 16, 41–58.

Eliopoulos, D., Economou, G., Tzifas, I., Papatrechas, C., 2014. The potential of rare earth elements in Greece. ERES 2014, 1st European Rare Earth Resources Conference, September 4–7, Milos, Greece, pp. 308–316.

Escuder Viruete, J., Díaz de Neira, A., Hernaiz Huerta, P.P., Monthel, J., García Senz, J., Joubert, M., Lopera, E., Ullrich, T., Friedman, R., Mortensen, J., Pérez-Estaún, A., 2006. Magmatic relationships and ages of Caribbean Island arc tholeiites, boninites and related felsic rocks, Dominican Republic. Lithos 90, 161–186.

Escuder Viruete, J., Pérez-Estaún, A., Contreras, F., Joubert, M., Weis, D., Ullrich, T.D., Spadea, P., 2007. Plume mantle source heterogeneity through time: insights from the Duarte Complex, Hispaniola, northeastern Caribbean. J. Geophys. Res. 112, B04203.

Freyssinet, P., Butt, C.R.M., Morris, R.C., 2005. Ore-forming processes related to lateritic weathering. Econ. Geol. 100th Anniversary Volume, pp. 681–722.

Frost, B.R., Evans, K.A., Swapp, S.M., Beard, J.S., Mothersole, F.E., 2013. The process of serpentinization in dunite from New Caledonia. Lithos 178, 24–39.

Galí, S., Proenza, J.A., Labrador, M., Tauler, E., Melgarejo, J.C., 2007. Numerical modelling of oxide-type Ni laterite deposits: preliminary results. In: Andrew, C.J., et al. (Eds.), Digging Deeper, 2. Irish Association of Economic Geology, pp. 1385–1388.

Gleeson, S.A., Butt, C.R., Elias, M., 2003. Nickel laterites: a review. SEG Newsl. 54, 11–18.

Golightly, J.P., 1981. Nickeliferous laterite deposits. Econ. Geol. 75th Anniversary Vol., pp. 710–735

Golightly, J.P., 2010. Progress in understanding the evolution of nickel laterites. Soc. Econ. Geol. Spec. Publ. 15, 451–485.

Golightly, J.P., Plamondon, M., Srivastava, R.M., 2008. 43-101F1 technical report on the Moa Occidental and Moa Oriental nickel laterite properties in Cuba: Prepared for Sherritt International Corporation accessed March 25, 2015, at, http://www.sedar.com/GetFile.do?lang=EN&docClass=24&issuerNo=00002460&fileName=/csfsprod/data88/filings/01240793/00000001/f%3A%5Crarcher%5C12941-0001%5C2007AIF%5C43-101report.pdf (102 pp.).

Grant, J.A., 1986. The isocon diagram—a simple solution to Gresens' equation for metasomatic alteration. Econ. Geol. 81, 1976–1982.

Grant, J.A., 2005. Isocon analysis: a brief review of the method and applications. Phys. Chem. Earth 30, 997–1004.

Gray, J.D., Schorin, K.H., Butt, C.R.M., 1996. Mineral associations of platinum and palladium in lateritic regolith, Ora Banda Sill, Western Australia. J. Geochem. Explor. 57, 245–255.

Gresens, R.L., 1967. Composition–volume relationships of metasomatism. Chem. Geol. 2, 47–55.

Haldemann, E.G., Buchan, R., Blowes, J.H., Chandler, T., 1979. Geology of lateritic nickel deposits, Dominican Republic. In: Evans, D.J.I., Shoemaker, R.S., Veltman, H. (Eds.), International Laterite Symposium. Amer. Inst. Mining, Metal., and Petroleum Engineers, New York, pp. 57–84.

Hein, J.R., Mizell, K., Koschinsky, A., Conrad, T.A., 2013. Deep-ocean mineral deposits as a source of critical metals for high- and green-technology applications: comparison with land-based resources. Ore Geol. Rev. 51, 1–14.

Iturralde-Vinent, M.A., Díaz Otero, C., Rodríguez Vega, A., Díaz Martínez, R., 2006. Tectonic implications of paleontologic dating of Cretaceous–Danian sections of Eastern Cuba. Geol. Acta 4, 89–102.

Janots, E., Bernier, F., Brunet, F., Muñoz, M., Trcera, N., Berger, A., Lanson, M., 2015. Ce(III) and Ce(IV) (re)distribution and fractionation in a laterite profile from Madagascar: insights from in situ XANES spectroscopy at the Ce LIII-edge. Geochim. Cosmochim. Acta 153, 134–148.

Jochum, K.P., Weis, U., Stoll, B., Kuzmin, D., Yang, Q., Raczek, I., Jacob, D.E., Stracke, A., Birbaum, K., Frick, D.A., Günther, D., Enzweiler, J., 2011. Determination of reference values for NIST SRM 610-617 glasses following ISO guidelines. Geostand. Geoanal. Res. 35, 397–429.

Johnson, D.B., du Plessis, C.A., 2015. Biomining in reverse gear: using bacteria to extract metals from oxidised ores. Miner. Eng. 75, 2–5.

Kooijman, E., Berndt, J., Mezger, K., 2012. U–Pb dating of zircon by laser ablation ICP-MS: recent improvements and new insights. Eur. J. Mineral. 24, 5–21.

Kalatha, S., Economou-Eliopoulos, M., 2015. Framboidal pyrite and bacterio-morphic goethite at transitional zones between Fe–Ni laterites and limestones: evidence from Lokris, Greece. Ore Geol. Rev. 65, 413–425.

Labrador, M., Proenza, J.A., Galí, S., Melgarejo, J.C., Tauler, E., Rojas-Purón, A.L., Muñoz-Gómez, N., Blanco-Moreno, J.A., 2007. In: Andrew, C.J. (Ed.), Supergene Co-Ni-Mn mineralization in Ni-laterite deposits from northeast Cuba. Digging Deeper, 2. Irish Assoc. Econ. Geol., pp. 1397–1400.

Laskou, M., Economou-Eliopoulos, M., 2007. The role of microorganisms on the mineralogical and geochemical characteristics of the Parnassos–Ghiona bauxite deposits, Greece. J. Geochem. Explor. 93, 67–77.

Lavaut, W., 1998. Tendencias geológicas del intemperismo de las rocas ultramáficas en Cuba oriental. Rev. Minera Geol. 15, 9–16.

Lazarenkov, V.G., Tikhomirov, B., Zhidkov, Y., Talovina, V., 2005. Platinum group metals and gold in supergene nickel ores of the Moa and Nikaro deposits (Cuba). Lithol. Miner. Resour. 40, 521–527.

Lázaro, C., Blanco-Quintero, I.F., Rojas-Agramonte, Y., Proenza, J.A., Núñez-Cambra, K., García-Casco, A., 2013. First description of a metamorphic sole related to ophiolite obduction in the northern Caribbean: geochemistry and petrology of the Güira de Jauco Amphibolite complex (eastern Cuba) and tectonic implications. Lithos 179, 193–210.

Lewis, J.F., Jiménez, J.G., 1991. Duarte complex in the La Vega–Jarabacoa–Janico Area, Central Hispaniola: geological and geochemical features of the sea floor during the early stages of arc evolution. In: Mann, P., Draper, G., Lewis, J.F. (Eds.), Geologic and Tectonic Development of the North America–Caribbean Plate Boundary in Hispaniola. Geol. Soc. Am. Spec. Paper 262, pp. 115–142.

Lewis, J.F., Draper, G., Proenza, J.A., Espaillat, J., Jiménez, J., 2006a. Ophiolite-related ultramafic rocks (serpentinites) in the Caribbean region: a review of their occurrence, composition, origin, emplacement and nickel laterite soils. Geol. Acta 4, 237–263.

Lewis, J.F., Escuder-Viruete, J., Hernaiz-Huerta, P.P., Gutiérrez, G., Draper, G., Pérez-Estaún, A., 2002. Subdivisión geoquímica del arco de Isla Circum-Caribeño, Cordillera Central Dominicana: Implicaciones para la formación, acreción y crecimiento cortical en un ambiente intraoceánico. Acta Geol. Hisp. 37, 81–122.

Lewis, J.F., Proenza, J.A., Jolly, W.T., Lidiak, E.G., 2006b. Monte del Estado (Puerto Rico) and Loma Caribe (Dominican Republic) peridotites: a look at two different Mesozoic mantle sections within northern Caribbean region. Geophys. Res. Abstr. 8, p. A-08798.

Liivamägi, S., Somelar, P., Mahaney, W.C., Kirs, J., Vircava, I., Kirsimäe, K., 2014. Late Neoproterozoic Baltic paleosol: intense weathering at high latitude? Geology 42, 323–326.

Linchenat, A., Shirakova, I., 1964. Individual characteristics of nickeliferous iron (laterite) deposits of the northeast part of Cuba (Pinares de Mayari, Nicaro and Moa). 24th International Geological Congress, Montreal, Part 14, Section 14, pp. 172–187.

Lithgow, E.W., 1993. Nickel laterites of central Dominican Republic Part I. Mineralogy and ore dressing. In: Reddy, R.G., Weizenbach, R.N. (Eds.), The Paul E. Queneau Int. Symposium, Extractive Metallurgy of Copper, Nickel and CobaltFundamental Aspects vol. I. The Minerals, Metals and Materials Society, Portland, pp. 403–425.

Little, B.J., Wagner, P.A., Lewandowski, Z., 1997. Spatial relationships between bacteria and mineral surfaces. In: Banfield, J.F., Nealson, K.H. (Eds.), Geomicrobiology: Interactions Between Microbes and Minerals. Reviews in Mineralogy 35, pp. 123–159.

Maier, W.D., Barnes, S.-J., Bandyayera, D., Livesey, T., Li, C., Ripley, E., 2008. Early Kibaran rift-related mafic–ultramafic magmatism in western Tanzania and Burundi: petrogenesis and ore potential of the Kapalagulu and Musongati layered intrusions. Lithos 101, 24–53.

Maksimović, Z.J., Pantó, G., 1996. Authigenic rare earth minerals in karst-bauxites and karstic nickel deposits. In: Jones, A.P., Wall, F., Williams, C.T. (Eds.), Rare Earth Minerals: Chemistry, Origin and Ore DepositsMineralogical Society Series 7. Chapman and Hall, London, pp. 257–279.

Marchesi, C., Garrido, C.J., Godard, M., Proenza, J.A., Gervilla, F., Blanco-Moreno, J., 2006. Petrogenesis of highly depleted peridotites and gabbroic rocks from the Mayarí–Baracoa Ophiolitic Belt (eastern Cuba). Contrib. Mineral. Petrol. 151, 717–736.

Marchesi, C., Garrido, C.J., Proenza, J.A., Konc, Z., Hidas, K., Lewis, J.F., Lidiak, E., 2012. Mineral and whole rock compositions of peridotites from Loma Caribe (Dominican Republic): insights into the evolution of the oceanic mantle in the Caribbean region. Geophys. Res. Abstr. 14, EGU2012–EGU12161.

Marsh, E.E., Anderson, E.D., 2011. Ni–Co laterite deposits. U.S. Geol. Surv. Open File Rep. 2011, 1259–1268.

Medaris, L.G., Singer, B.S., Dott Jr., R.H., Naymark, A., Johnson, C.M., Schott, R.C., 2003. Late Paleoproterozoic climate and tectonics in southern Lake Superior region and Proto-North America: evidence from Baraboo interval quartzites. J. Geol. 111, 243–257.

Meyer, F.M., Happel, U., Hausberg, J., Wiechowski, A., 2002. The geometry and anatomy of the Los Pijiguaos bauxite deposit, Venezuela. Ore Geol. Rev. 20, 27–54.

Mongelli, G., 1997. Ce-anomalies in the textural components of Upper Cretaceous karst bauxites from the Apulian carbonate platform (southern Italy). Chem. Geol. 140, 69–79.

Naldrett, A.J., Duke, J.M., 1980. Platinum metals in magmatic sulfide ores. Science 208, 1417–1428.

Ndjigui, P.D., Bilong, P., 2010. Platinum-group elements in the serpentinite lateritic mantles of the Kongo–Nkamouna ultramafic massif (Lomié region, South-East Cameroon). J. Geochem. Explor. 107, 63–76.

Nelson, C.E., Proenza, J.A., Lewis, J.F., López-Kramer, J., 2011. The metallogenic evolution of the Greater Antilles. Geol. Acta 9, 229–264.

Platina Resources, 2015. Excellent Testwork Results from Owendale Scoping Study Available at: http://www.platinaresources.com.au/files/announcements/2015_01_20_-_PGM_ASX_-_Owendale_Scoping_Study.pdf (Accessed 25 March 2015).

Pol, A., Barends, T.R.M., Bietl, A., Khadem, A.F., Eygensteyn, J., Jetten, M.S.M., Op den Camp, H.J.M., 2014. Rare earth metals are essential for methanotrophic life in volcanic mudpots. Environ. Microbiol. 16, 255–264.

Proenza, J.A., Gervilla, F., Melgarejo, J.C., 1999b. La Moho Transition Zone en el Macizo Ofiolítico Moa–Baracoa: un ejemplo de interacción magma/peridotite. Rev. Soc. Geol. Esp. 12, 309–327.

Proenza, J.A., Gervilla, F., Melgarejo, J.C., Bodinier, J.L., 1999a. Al- and Cr-rich chromitites from the Mayarí–Baracoa Ophiolitic Belt (Eastern Cuba): consequence of interaction between volatile-rich melts and peridotite in suprasubduction mantle. Econ. Geol. 94, 547–566.

Proenza, J.A., Roqué, J., Labrador, M., Galí, S., Tauler, E., Gallardo, T., Lewis, J.F., Longo, F., 2010. Mineralogical composition and mineral chemistry of supergene cobalt ores from eastern Cuba and Dominican Republic Ni-laterite deposits. 20th general meeting of the IMA, 21-27 August 2010, Budapest Hungary.

Proenza, J.A., Tauler, E., Melgarejo, J.C., Gali, S., Labrador, M., Marrero, N., Perez-Nelo, N., Rojas-Puron, A.L., Blanco-Moreno, J.A., 2007a. Mineralogy of oxide and hydrous silicate Ni laterite profiles in Moa Bay area, northeast Cuba. In: Andrew, C.J., et al. (Eds.), Digging Deeper, 2. Irish Association of Economic Geology, pp. 1389–1392.

Proenza, J.A., Zaccarini, F., Lewis, J., Longo, F., Garuti, G., 2007b. Chromian spinel composition and platinum-group mineral assemblage of PGE-rich Loma Peguera chromitites, Loma Caribe peridotite, Dominican Republic. Can. Mineral. 45, 211–228.

Proenza, J.A., Díaz-Marínez, R., Iriondo, A., Marchesi, C., Melgarejo, J.C., Gervilla, F., Garrido, C.J., Rodríguez-Vega, A., Lozano-Santacruz, R., Blanco-Moreno, J.A., 2006. Primitive Cretaceous island-arc volcanic rocks in eastern Cuba: the Téneme Formation. Geol. Acta 4, 103–121.

Redwood, S., 2014. Gold surge mining is booming in the Dominican Republic as investors follow the gold rush. Min. J. 24, 23–27.

Roqué-Rosell, J., Mosselmans, J.F.W., Proenza, J.A., Labrador, M., Galí, S., Atkinson, K.D., Quinn, P.D., 2010. Sorption of Ni by "lithiophorite–asbolane" intermediates in Moa Bay lateritic deposits, Eastern Cuba. Chem. Geol. 275, 9–18.

Rudashevsky, N.S., Rudashevsky, V.N., 2006. Patent of Russian Federation #2281808, Invention "Hydraulic Classifier", Moscow, 20 August 2006.

Rudashevsky, N.S., Rudashevsky, V.N., 2007. Patent of Russian Federation #69418, Industrial (Useful) Model, "Device for Separation of Solid Particles", Moscow, December 27, 2007.

Rudashevsky, N.S., Lupal, S.D., Rudashevsky, V.N., 2001. The Hydraulic Classifier. Russia Patent N 2165300, Patent Cooperation Treaty PCT/RU01/00123 (Moscow: 20 April 2001; 10 May 2001) (in Russian and English).

Sherritt, 2012. Sherrit International Corporation. 2012 Annual Report. Available at:, http://www.sherritt.com/getattachment/7a7b0634-0dd4-46c4-bcda-19d73042fa9c/2012-Annual-Report (Accessed 25.03.2015).

Simandl, G.J., 2014. Geology and market-dependent significance of rare earth element resources. Mineral. Deposita 49, 889–904.

Terekhov, D.S., Nanthakumar, V.E., 2013. Direct extraction of nickel and iron from laterite ores using carbonyl process. Miner. Eng. 54, 124–130.

Trincal, V., Charpentier, D., Buatier, M.D., Grobety, B., Lacroix, B., Labaume, P., Sizun, J.P., 2014. Quantification of mass transfers and mineralogical transformations in a thrust fault (Monte Perdido thrust unit, southern Pyrenees, Spain). Mar. Pet. Geol. 55, 160–175.

Tsikouras, B., Karipi, S., Rigopoulos, I., Perraki, M., Pomonis, P., Hatzipanagiotou, K., 2009. Geochemical processes and petrogenetic evolution of rodingite dikes in the ophiolite complex of Othrys (Central Greece). Lithos 113, 540–554.

USGS, 2013. Mineral commodity summaries 2013. Available at:, http://minerals.usgs.gov/minerals/pubs/mcs/2013/mcs2013.pdf (Accessed 25.03.2015).

Villanova-de-Benavent, C., Proenza, J.A., Galí, S., García-Casco, A., Tauler, E., Lewis, J.F., Longo, F., 2014. Garnierites and garnierites: textures, mineralogy and geochemistry of garnierites in the Falcondo Ni laterite deposit, Dominican Republic. Ore Geol. Rev. 58, 91–109.

Vodyanitskii, Y.N., 2010. Iron hydroxides in soils: a review of publications. Eurasian Soil Sci. 43, 1244–1254.

Wang, W., Pranolo, Y., Cheng, C.Y., 2011. Metallurgical processes for scandium recovery from various resources: a review. Hydrometallurgy 108, 100–108.

Wilde, A., Edwards, A., Yakubchuk, A., 2003. Unconventional deposits of Pt and Pd: a review with implications for exploration. SEG Newsletter 52, 1 and 10–18.